



Published in final edited form as:

*Neuroimage*. 2021 January 15; 225: 117457. doi:10.1016/j.neuroimage.2020.117457.

## Postsynaptic activity of inhibitory neurons evokes hemodynamic fMRI responses

Alexander John Poplawsky<sup>a</sup>, Bistra Iordanova<sup>b</sup>, Alberto L. Vazquez<sup>a,b</sup>, Seong-Gi Kim<sup>c,d</sup>, Mitsuhiro Fukuda<sup>a,\*</sup>

<sup>a</sup>Department of Radiology, University of Pittsburgh, Pittsburgh, PA 15203, United States

<sup>b</sup>Department of Bioengineering, University of Pittsburgh, Pittsburgh, PA 15203, United States

<sup>c</sup>Center for Neuroscience Imaging Research, Institute for Basic Science, Suwon 440-330, Korea

<sup>d</sup>Department of Biomedical Engineering, Sungkyunkwan University, Suwon, 440-330, Korea

### Abstract

Functional MRI responses are localized to the synaptic sites of evoked inhibitory neurons, but it is unknown whether, or by what mechanisms, these neurons initiate functional hyperemia. Here, the neuronal origins of these hemodynamic responses were investigated by fMRI or local field potential and blood flow measurements during topical application of pharmacological agents when GABAergic granule cells in the rat olfactory bulb were synaptically targeted. First, to examine if postsynaptic activation of these inhibitory neurons was required for neurovascular coupling, we applied an NMDA receptor antagonist during cerebral blood volume-weighted fMRI acquisition and found that responses below the drug application site (up to ~1.5 mm) significantly decreased within ~30 min. Similarly, large decreases in granule cell postsynaptic activities and blood flow responses were observed when AMPA or NMDA receptor antagonists were applied. Second, inhibition of nitric oxide synthase preferentially decreased the initial, fast component of the blood flow response, while inhibitors of astrocyte-specific glutamate transporters and vasoactive intestinal peptide receptors did not decrease blood flow responses. Third, inhibition of GABA release with a presynaptic GABA<sub>B</sub> receptor agonist caused less reduction of neuronal and blood flow responses compared to the postsynaptic glutamate receptor antagonists. In conclusion, local hyperemia by synaptically-evoked inhibitory neurons was primarily driven by their postsynaptic activities, possibly through NMDA receptor-dependent calcium signaling that was not wholly dependent on nitric oxide.

This is an open access article under the CC BY-NC-ND license (<http://creativecommons.org/licenses/by-nc-nd/4.0/>)

\*Corresponding author. mif5@pitt.edu (M. Fukuda).

Credit authorship contribution statement

**Alexander John Poplawsky:** Conceptualization, Methodology, Investigation, Formal analysis, Writing - original draft, Visualization. **Bistra Iordanova:** Investigation, Writing - review & editing, Visualization. **Alberto L. Vazquez:** Writing - review & editing, Funding acquisition. **Seong-Gi Kim:** Conceptualization, Writing - review & editing, Funding acquisition. **Mitsuhiro Fukuda:** Conceptualization, Methodology, Investigation, Formal analysis, Writing - original draft, Visualization, Funding acquisition.

Declaration of Competing Interest

The authors declare they have no competing financial interests.

Data and code availability statement

The data and code described in this study are available from the corresponding author upon reasonable request.

## Keywords

BOLD; CBF; CBV; GABAergic neurons; Neurovascular coupling

---

## 1. Introduction

Functional MRI (fMRI) noninvasively examines in vivo brain function in humans and animals by measuring the hemodynamic response to neuronal activity. Due to its indirect nature, it is important to understand how neurons couple to the vasculature. In particular, studying how GABAergic neurons are involved in functional hyperemia has been of growing interest because these neurons co-release vasoactive neurotransmitters (Cauli et al., 2004; for review see, Hamel, 2006) and have a close apposition to blood vessels (Kocharyan et al., 2008; Vaucher et al., 2000). In addition, GABAergic neurons are genetically and functionally diverse (Taniguchi, 2014), making their roles in neurovascular coupling complex and in need of further study.

Neurovascular coupling has been traditionally examined in sensory cortical areas (Boorman et al., 2010; Devor et al., 2008; Enager et al., 2009; Lecrux et al., 2011; Lee et al., 2010), where sensory input is integrated through complex laminar connections and involves a diversity of neuron types (Logothetis, 2008). Consequently, in these models, both excitatory and inhibitory neurons are often dependently activated, making it difficult to separate the unique role of inhibitory neurons to functional hyperemia. For this reason, optogenetics has been used to selectively stimulate inhibitory neurons (Urban et al., 2012; Zhao et al., 2011). With this technique, light-sensitive ion channels, like channelrhodopsin-2 (ChR2), were genetically targeted to specific inhibitory neuron populations and their selective contributions to hemodynamic responses were examined (Anenberg et al., 2015; Dahlqvist et al., 2020; Krawchuk et al., 2020; Lee et al., 2020a, Lee et al., 2020b; Uhlirva et al., 2016; Vazquez et al., 2018). These studies showed that light-evoked GABAergic activity can increase or decrease blood flow and blood volume responses. However, recent evidence suggested that blood vessel dilation (Rungta et al., 2017) and neuronal circuit dynamic changes (Mahn et al., 2016; Oceau et al., 2019; Owen et al., 2019; Raimondo et al., 2012) can also be directly affected by the light stimulus. In addition, ChR2 is nonspecifically distributed throughout the membrane of neurons (Iordanova et al., 2018, 2015) and is not exclusively localized to the synapse. Since neurovascular coupling pathways seem to be compartmentalized to the synaptic microdomain (Poplawsky et al., 2015), globally distributed light-sensitive channels may contribute to other nonspecific or confounding responses, especially if the ion channel is permeable to calcium, like ChR2 (Nagel et al., 2003). There was some indirect evidence for the involvement of synaptically-activated inhibitory neurons to increased blood flow in the cerebellar cortex (Mathiesen et al., 1998), but further study is necessary. To examine these issues here, we preferentially evoked GABAergic neuronal activity through dendrodendritic synapses in the main olfactory bulb of isoflurane-anesthetized rats and measured the cerebral blood volume-weighted (CBVw) fMRI responses.

The olfactory bulb is an advantageous model because it has well-established circuitry that allows targeted synaptic stimulation of inhibitory neurons. Specifically, the apical dendrites of GABAergic granule cells connect to the lateral dendrites of excitatory mitral (and tufted) cells in the external plexiform layer (EPL) via reciprocal dendrodendritic synapses (Bartel et al., 2015; Price and Powell, 1970; Rall and Shepherd, 1968), which mediate lateral inhibition and regulate excitatory spread along mitral cell dendrites (Luo and Katz, 2001; Xiong and Chen, 2002; Yokoi et al., 1995). Importantly, preferential activation of these inhibitory neurons has been shown with antidromic stimulation of the lateral olfactory tract (LOT), which contain the mitral cell axons (Jahr and Nicoll, 1980; Mori and Takagi, 1978; Rall et al., 1966). Local field potentials (LFPs) evoked by LOT stimulation have a signature waveform indicating the excitation of inhibitory granule cells (Nakashima et al., 1978; Nicoll, 1969; Uva et al., 2006), and current source density analyses of laminar LFPs revealed a localized current sink (i.e. synaptic depolarization) in EPL (Aroniadou-Anderjaska et al., 1999; Poplawsky et al., 2015; Uva et al., 2006). Optical imaging with a voltage sensitive dye, indicative of synaptic potential changes, was also confined to EPL following LOT stimulation (Laris et al., 2007). It was further shown that depolarization of the lateral dendrites of mitral cells released glutamate onto the dendritic spines of granule cells, followed by reciprocal release of GABA onto the mitral cell dendrites (Chen et al., 2000; Halabisky et al., 2000; Isaacson and Strowbridge, 1998; Schoppa et al., 1998). Activation of dendrodendritic synapses by LOT stimulation also dilated microvessels near the site of synaptic activity, which we demonstrated with CBVw fMRI. Namely, we observed fMRI responses specifically localized to EPL with an approximate 100- $\mu$ m spread beyond this layer (Poplawsky et al., 2019a, 2015). In the present study, we examine whether postsynaptic GABAergic neuronal activity is required for these hemodynamic responses evoked by LOT stimulation.

Previous examinations of the pre- or post-synaptic origins of the hemodynamic response in olfactory bulb glomeruli in the glomerular layer (GL) are controversial. Some studies suggested that presynaptic glutamate release alone and its detection by astrocytes through glutamate transporters or mGluR5 can initiate functional hyperemia (Gurden et al., 2006; Petzold et al., 2008; see also Zhao et al., 2017), while other studies showed that postsynaptic activity was required (Chaigneau et al., 2007; De Saint Jan and Westbrook, 2005; Otsu et al., 2015). However, in these studies, both excitatory and inhibitory neurons were elicited, similar to the aforementioned sensory cortical regions; and the complexity caused by this mixture of evoked neuronal populations could explain the observed discrepancies. In the current study, our established LOT-stimulation model simplifies this neuronal circuit by isolating the contributions of inhibitory neurons to the hemodynamic response. Therefore, we aimed to test whether our observed CBVw-fMRI responses to LOT stimulation were caused by presynaptic glutamate release alone or whether postsynaptic activity of inhibitory granule cells was necessary. For this, we applied various pharmacological agents to the bulb surface during fMRI recording and, in separate experiments, during optical blood flow and electrophysiological measurements.

## 2. Materials and methods

Experiments consisted of three parts: (1) confirmation with c-Fos immunohistochemistry, (2) pharmacological tests of CBVw-fMRI responses, and (3) pharmacological tests of neuronal activity and optical blood flow responses. LFPs were measured with a metal microelectrode; blood flow was measured with laser-Doppler flowmetry (LDF); total hemoglobin content-weighted images were measured with optical intrinsic signal imaging (OISI); and CBVw fMRI was achieved with a monocrySTALLINE iron oxide nanoparticle (MION) contrast agent. All data were analyzed with MATLAB (MathWorks, Natick, MA, USA), unless otherwise noted. LFPs, LDF, and OISI data were averaged over multiple runs with identical stimulus conditions before further analyses. Analyses were performed on each rat separately before group averaging. Experimental procedures were previously described in detail (Poplawsky et al., 2015).

### 2.1. Animal preparation

A total of 56 male Sprague Dawley rats (isoflurane-anesthetized, freely breathing,  $311.0 \pm 61.6$  g; mean  $\pm$  SD) were used in our study with approval from the University of Pittsburgh Institutional Animal Care and Use Committee in accordance with the standards for humane animal care and use as set by the Animal Welfare Act and the National Institutes of Health's *Guide for the Care and Use of Laboratory Animals*. No rats had time-locked heart rate or blood pressure changes to LOT stimulation, while two rats were removed from the study due to unstable blood pressures.

For all surgical procedures, rats were induced and maintained with 5.0% and 2.0% isoflurane, respectively; while all functional studies were performed at least 60 min after decreasing the isoflurane to 1.1–1.4%. The isoflurane level remained constant for individual subjects during all recordings. We chose isoflurane in this study because it is relatively easy to maintain a stable, long-term physiological condition (Masamoto et al., 2007), as opposed to  $\alpha$ -chloralose in our previous studies (Poplawsky et al., 2019a, 2015). The skull over the right olfactory bulb was removed ( $\sim 3$  mm  $\times$  2 mm) while keeping the dura intact. A dental cement well with inlet (for both fMRI and non-fMRI experiments) and outlet (for fMRI experiment only) tubes (PE-50) was built around the craniotomy for superfusion. The craniotomy was filled with saline, covered with an acrylic plate (1.5 mm thick) and sealed with dental cement for fMRI experiments, while it remained open for non-fMRI experiments. A stimulation electrode was stereotaxically implanted into LOT (Mode, A0.2, L4.2, D8.5) for all animals ( $n = 56$ ). The final stimulation electrode position was determined by local field potentials (LFPs) evoked by LOT stimulation in the olfactory bulb. An Ag/AgCl reference electrode was placed over the left visual cortex between the dura and bone. The left femoral artery was catheterized for blood pressure and heart rate monitoring, and the left femoral vein for contrast agent and continuous 5% dextrose fluid administration (1.0 mL/kg/h). The mean arterial blood pressure was maintained between 70 and 130 mmHg. Atropine (0.05 mg/kg, i.m.) was administered at the beginning and end of surgery. A respiratory pillow was placed under the chest for breathing rate measurements and a warm-water circulator (for fMRI) or an electric heating pad (for non-fMRI) with rectal temperature feedback was used to maintain the core body temperature at  $37 \pm 1$  °C. Rats freely breathed

a 0.75–0.95 L/min air and 0.09–0.12 L/min oxygen gas mixture through a nose cone that maintained oxygen levels between 28 and 29% (Capnomac Ultima capnometer, Datex-Engstrom, Helsinki, Finland).

## 2.2. Confirmation with c-Fos immunohistochemistry

We used cell-specific molecular markers to histologically identify neurons activated by LOT stimulation. We performed double immunostaining for nuclear c-Fos, a marker for increased cellular activity, and glutamic acid decarboxylase (GAD<sub>67</sub>), a marker for GABAergic neurons, to examine the degree of their co-localization ( $n = 4$  rats). C-Fos is a nuclear transcription factor and an established functional marker of activated neurons (Dragunow and Faull, 1989; Kovacs, 1998). LOT was stimulated every 60 s ( $n = 3$ ) or 30 s ( $n = 1$ ) by a 10-s pulse train (100- $\mu$ s pulse width,  $-150$  –  $-200$   $\mu$ A current intensity, 40 Hz) using an isolator (Isoflex, AMPI, Israel) equipped with an electrical pulse generator (Master 9, AMPI, Israel) for a total of 90 min. Then, the rat was deeply anesthetized with Euthanasia-III Solution (0.2 mL, i.p., *active ingredients*: 390-mg pentobarbital sodium and 50-mg phenytoin sodium per mL, Med-Pharmex Inc., Pomona, CA) and perfused transcardially with phosphate buffered saline (PBS, 0.01 M, pH 7.4) followed by 4% paraformaldehyde in PBS. The brain was removed and stored in 30% sucrose in PBS at 4 °C for cryoprotection and then flash-frozen and stored at  $-80$  °C. Frozen brain tissue was cryosectioned using a Leica CM1850 cryostat (Leica, Wetzlar, Germany) in 25- $\mu$ m-thick slices, and mounted on glass slides. For c-Fos expression, the sections were incubated in a primary polyclonal rabbit antibody (SC-52, 1:200 Santa Cruz Biotechnology Inc., Dallas, Texas, USA) followed by Alexa Fluor 488 goat anti-rabbit secondary antibody (A-11008, 1:500, Invitrogen, Waltham, Massachusetts, USA). To identify inhibitory cell populations, we used GAD<sub>67</sub> mouse monoclonal antibody (1:200, MAB5406, Millipore, St. Louis, MO, USA) followed by Alexa Fluor 594 donkey anti-mouse secondary antibody (R37115, 1:500, Invitrogen). To assist in layer identification, cytoarchitectonic boundaries were visualized by staining nuclei with Hoechst 33342 (H3570, Invitrogen). All four rats were visually inspected by a fluorescence microscope. In one representative rat (30-s interstimulus interval), immunohistochemical-stained sections were imaged with a confocal microscope (FluoView 1000, Olympus, Inc., Tokyo, Japan) at a  $0.621 \mu\text{m} \times 0.621 \mu\text{m}$  pixel resolution and  $20 \times$  magnification (Fig. 1B). A threshold was applied to the c-Fos image to identify this nuclear-specific fluorescence.

## 2.3. Pharmacological tests on CBVw-fMRI responses

CBVw-fMRI responses evoked by LOT stimulation were recorded and compared during the 60-min pre-drug control, 90-min drug application, and 180-min recovery (i.e., after washout of the drug) periods (Figs. 2 and 3). We chose a contrast-enhanced CBVw method, instead of BOLD, due to its higher specificity to the sites of synaptic activity changes (Poplawsky et al., 2019a), which was similarly shown in non-invasive CBVw fMRI studies of humans (Huber et al., 2017; Lu et al., 2003). LOT was repeatedly stimulated for 64 s at 40 Hz (200- $\mu$ s pulse width,  $-200$ - $\mu$ A current intensity) every 304 s for the entirety of the pharmacological experiment. Despite the technical challenge (Aksenov et al., 2019), we chose topical application because systemic injection of drugs (e.g., Schoppa et al. (1998); Zhao et al. (2017)) may act at sites normally not involved in LOT stimulation and the precise sites of drug action cannot be known. We targeted NMDA instead of AMPA receptors

because their activation was required for dendrodendritic inhibition (Isaacson and Strowbridge, 1998; Schoppa et al., 1998) and  $\text{Ca}^{2+}$  influx through NMDA receptors was important for GABA release in EPL (Chen et al., 2000; Halabisky et al., 2000). Further, reduction of mitral cell glutamate release by presynaptic NMDA receptor antagonists was expected to be negligible (Aroniadou-Anderjaska et al., 1999; Sassoe-Pognetto and Ottersen, 2000).

### 2.3.1. Remote drug application simultaneous with CBVw-fMRI acquisition—

For topical drug application during fMRI, we removed the skull over the right bulb and fixed 1.5-m inlet and 0.1-m outlet tubes at opposite ends of the craniotomy to apply and remove the drug, respectively (Fig. 2A). The preparation was filled with saline and sealed with a 1.5-mm thick acrylic plastic window with special attention made to remove all air. A surface coil (10-mm diameter, transmit and receive) was placed over the bulb before the rat was positioned to the magnet isocenter (9.4-T/31-cm MR system interfaced by a DirectDrive console, Agilent Tech, Santa Clara, CA; actively shielded gradient coil with 40-G/cm peak gradient strength and 120- $\mu$ s rise time, Magnex, UK). Outside of the magnet, a reservoir of 1-mL PBS vehicle or PBS containing the drug was gravity-fed to the bulb surface through the inlet tube. Liquid exiting the bulb was collected in a second reservoir near the head of the rat.

T2-weighted anatomical (fast spin-echo sequence, 5-s TR, 40.7-ms effective TE, train of 4 echoes,  $8 \times 8 \text{ mm}^2$  FOV,  $128 \times 128$  matrix, 9 slices, 0.5 mm slice thickness) and CBVw-fMRI images (compressed-sensing GRE sequence (Zong et al., 2014), 125-ms TR, 8-ms TE, same FOV,  $64 \times 64$  matrix, reduction factor of 4, 2-s effective temporal resolution,  $35^\circ$  flip angle) were acquired. The compressed-sensing GRE sequence was chosen to reduce the susceptibility artifacts caused by air sinuses near the olfactory bulb, while increasing our temporal resolution. For CBVw-fMRI contrast, a single i.v. bolus of Feraheme (15 mg Fe/kg, ferumoxytol, AMAG Pharmaceuticals, MA, MION) was injected; in addition to a continuous maintenance dose. The rate of continuous MION delivery ( $\sim 1 \text{ mg/kg}$  per 0.1 mL saline-diluted solution, i.v.) was varied so that the baseline fMRI signal in the bulb was constant throughout the experiment. No BOLD fMRI images were acquired. During acquisition, a single fMRI run consisted of 120-s off, 64 s of LOT stimulation, and 120-s off ( $\sim 5 \text{ min/run}$ ). LOT was repeatedly stimulated in this way during the pharmacological study with 3–7 baseline runs to establish a steady-state to stimulation, followed by vehicle infusion and 12–15 pre-drug control runs, drug infusion and 18 drug applied runs ( $\sim 90 \text{ min}$ ), and three vehicle washout infusions spaced 10-min apart and 35 recovery runs ( $\sim 180\text{-min}$ ). Runs during infusions were excluded from analysis along with a total of five other runs that had various complications identified prior to analysis (e.g., reconstruction error). Following acquisition, images were reconstructed using a k-t FOCUSS algorithm with a Karhunen-Loeve sparsifying transform (Zong et al., 2014). Functional MRI time series were motion corrected with SPM12 (Wellcome Trust centre for Neuroimaging, London, UK).

**2.3.2. Primary GLM—**The CBVw-fMRI response evoked by LOT stimulation has a unique time course with two distinct phases: 1) an initial, fast CBV increase that decreases toward baseline within the first 10 s of the stimulus and 2) a slower activation that slowly

builds throughout the 64-s stimulation (Poplawsky et al., 2015). Therefore, we used an average time course of the fMRI response to the same stimuli from preliminary studies as a predictor variable; in addition to six motion correction values (3 translation, 3 rotation) calculated in SPM12 and linear drift covariates. The response variable was either single LOT stimulation trials or concatenated trials representing the pre-drug control, drug applied, and recovery experimental conditions. Percent change and t-maps were calculated in SPM12 for display and statistical thresholding, respectively.

**2.3.3. Spatial mapping of APV effects using linear regression analysis—**A second, finite impulse response GLM analysis was performed in SPM12 to determine the spatial extent of the changes in the evoked fMRI responses due to the drug application and recovery in a voxel-wise manner. Here, the response variable was the fMRI percent change maps to individual fMRI runs of LOT stimulations in time (~5 min/run), calculated in the primary GLM analysis, and the predictor variable was the drug application and washout block schedule. The drug schedule block design used for analysis had 12–18 pre-drug control “off” fMRI runs, 17 drug applied “on” runs, and 31–32 recovery “off” runs. We also included a linear drift covariate and calculated the percent change and t-value maps for each rat.

## 2.4. Pharmacological tests on neuronal activity and blood flow responses

**2.4.1. Optical intrinsic signal imaging—**In a subset of animals ( $n = 8$ ), OISI was performed before drug administration at a hemoglobin isosbestic point simultaneous with LDF measurements to compare blood volume and blood flow responses evoked by LOT stimulation, respectively (Fig. 4, A–D). Each run consisted of a 120-s pre-stimulus baseline, 64-s LOT stimulation (100- $\mu$ s pulse width, –200- $\mu$ A current intensity, 40 Hz pulse train), and 120-s post-stimulus periods, unless otherwise noted. For OISI, five runs were repeated and averaged. The bulb surface was illuminated by oblique light guides connected to a halogen light source (250 W, Research QTH Light Source, Thermo-Oriel, Stratford, CT, USA) that transmitted filtered light at a wavelength of  $600 \pm 50$  nm. Images of the remitted light were captured by a camera through a barrier filter ( $572 \pm 14$  nm) to obtain blood volume weighted signals (Vazquez et al., 2014). OIS images were acquired over a  $3.7 \times 3.2 - 4.7 \times 4.1$  mm<sup>2</sup> FOV, depending on the microscope magnification, at 30 frames per second (fps) using an analog frame acquisition board (Corona-II, Matrox Electronic Systems Ltd., Dorval, Quebec, Canada) and an analog CCD camera (XC-ST70, 640  $\times$  480 pixels,  $11.6 \times 13.5$   $\mu$ m<sup>2</sup> / pixel, Sony, Japan) on an *epi*-fluorescence microscope equipped with a  $1 \times (0.25$  NA) objective (MVX-10; Olympus, Tokyo, Japan). To accelerate post-processing, a  $2 \times 2$  binning and 15-frame averaging (i.e., 0.5 s per frame = 15 frames / 30 fps) were performed on the images. To generate activation maps of blood volume responses, first, a baseline image ( $R$ ) was obtained by averaging images over the 120 s prior to stimulation. Differential images ( $\Delta R$ ) were then calculated by subtracting the baseline image from each image in time. Lastly, activation maps ( $\Delta R/R$ ) were generated by dividing the differential images by the baseline image (Fig. 4, B and C). To compare OISI and LDF time courses, the average OISI signal from a circular region of approximately 100- $\mu$ m in diameter (10 pixels) was chosen in the vicinity of the LDF probe tip. Then, relative OISI changes (%) to the baseline (averaged over 1 s before stimulus onset, equivalent to 2 frames) were calculated (Fig. 4D).

**2.4.2. Drugs**—Six drugs were used to evaluate the contribution of postsynaptic GABAergic neurons to the evoked blood flow responses. DL-2-Amino-5-phosphonopentanoic acid (APV), N $\omega$ -Nitro-L-arginine (L-NNA), and ( $\pm$ )-Baclofen (Baclofen) were purchased from Sigma (MilliporeSigma, St. Louis, MO). 2,3-Dioxo-6-nitro-1,2,3,4-tetrahydrobenzo[f]quinoxaline-7-sulfonamide disodium salt (NBQX), Dihydrokainic acid (DHK), and Vasoactive Intestinal Peptide Fragment 6–28 human, rat, porcine, bovine (VIP (6–28)) were purchased from Tocris Bioscience (Bio-Techne Corporation, Minneapolis, MN). All drugs were prepared in PBS (0.01 M, pH = 7.4), unless otherwise noted. APV was dissolved in saline by adding 0.1 M and 1 M NaOH and the final pH was adjusted to 7.4 by further adding 0.1 M NaOH. Baclofen was prepared in either PBS or artificial cerebrospinal fluid (126-mM NaCl, 2.5-mM KCl, 1-mM MgSO<sub>4</sub>•7H<sub>2</sub>O, 2-mM CaCl<sub>2</sub>•2H<sub>2</sub>O, 1.25-mM NaH<sub>2</sub>PO<sub>4</sub>•H<sub>2</sub>O, 26-mM NaHCO<sub>3</sub>, 10-mM D-glucose, 10-mM HEPES, bubbled with a mixture of 5% CO<sub>2</sub> and 95% O<sub>2</sub>, pH = 7.4). All drugs were topically applied to the dorsal surface of the right olfactory bulb with dura intact. Each rat underwent only one drug exposure to avoid possible drug interactions. Final concentrations of the drugs were adjusted to 25 mM for APV, 5 mM for NBQX, 1 mM for DHK, 1 mM for L-NNA, 0.1 mM for VIP (6–28) and 10 mM for Baclofen. These concentrations were based on previous reports: Gurden et al. (2006) for APV, NBQX, and baclofen; Petzold et al. (2008) for DHK; Akgören et al. (1997) for L-NNA; Lecrux et al. (2011) for VIP(6–28). For APV, we used 25 mM instead of 50 mM (Gurden et al., 2006) because a longer exposure time (> 120 min) with the higher concentration caused instability in the baseline LDF signal. For this in vivo study, a long drug application period was chosen to ensure deeper drug penetration to EPL through an intact dura mater and to elicit widespread effects measurable by LDF and fMRI. The efficiency of drug removal through washout depends on the time of drug exposure and washout, as well as on chemical properties like water solubility, lipid affinity, concentration, receptor-binding and -release kinetics, etc. Because the primary goal of the washout period was to control for time-dependent confounds not specific to the drug effects rather than to achieve complete recovery to baseline levels, the pre-drug control and washout periods were not statistically tested.

**2.4.3. LFP and LDF signal recordings**—LFP and LDF responses evoked by LOT stimulation were recorded from the granule cell layer (GCL) and the dorsal surface of the bulb, respectively. For baseline neuronal activity assessment, LFP was also recorded from the external plexiform layer (EPL). LOT was stimulated for 4–6 runs and averaged, with the exception of DHK experiments whereby LOT and odor stimulations were interleaved (64 s duration, every 608 s for each). Odor stimulation was performed by a custom-built olfactometer (Poplawsky and Kim, 2014). Briefly, solenoid valves diverted airflow (0.2 L/min medical gas, 21% O<sub>2</sub> and 79% N<sub>2</sub>) to one of two plastic bottles containing 100 mL of 5% (w/w) 2-hydroxyacetophenone (2HA) in mineral oil or 100 mL of 100% mineral oil. A Teflon tube with a one-way check valve was connected to the output of each bottle. These two lines converged onto a single Teflon tube with a one-way check valve that then merged with the isoflurane delivery line (1.0 L/min medical gas + 0.12 L/min O<sub>2</sub>) at the rat nose cone. Therefore, the effective concentration of 2HA was ~0.8% (w/w). A vacuum line at the opposite end of the nose cone removed the odors.

For APV ( $n = 8$  rats), L-NNA ( $n = 7$  rats), VIP (6–28) ( $n = 6$  rats), and baclofen ( $n = 9$  rats), the evoked responses to LOT stimulation were recorded from ~90 to 120 min after drug administration; ~60 to 90 min for NBQX ( $n = 6$  rats) due to a faster suppression of evoked LFPs; and ~90 to 150 min for DHK ( $n = 7$  rats) due to the acquisition of additional odor responses. Washout of the drug was performed only if suppression of the evoked responses was observed. Recovery, if taken, was recorded ~120–180 min after washout of the drugs.

For evoked LFP quantification, averaged data across runs were fully rectified and summed over the 64-s stimulation period. The summed LFP data were then divided by the sampling rate (10 kHz). For evoked LDF quantification, averaged data across runs were low-pass filtered with a 2-Hz cut-off frequency, and differences (LDF) from their baseline value (averaged over the 120-s pre-stimulus period) were obtained. Finally, LDF signals were summed during the stimulation periods, and divided by the data sample rate (1 kHz) to evaluate the magnitude of the evoked blood flow responses.

**2.4.4. Baseline neuronal activity assessment**—We used a 500-ms period prior to the stimulus onset in the LFP recordings obtained from EPL to assess baseline activity. In each rat, power spectra were computed for each condition using a multi-taper method with a time-bandwidth product of 3 and 5 tapers found in the Chronux MATLAB toolbox (<http://chronux.org>). The 60-Hz line noise was removed with the Chronux `rmlinesc` function. The spectra were then divided into delta (1–4 Hz), theta (4–8 Hz), alpha (8–13 Hz), beta (13–30 Hz), and gamma (30–90 Hz) bands and the sum of the powers was obtained for each band. All of the frequency bands were then compared before and after drug administration and, if different, the gamma band was further examined because it correlates well with hemodynamic responses (Logothetis et al., 2001; Nielsen and Lauritzen, 2001; Viswanathan and Freeman, 2007).

## 2.5. Group statistics

GraphPad Prism (version 8.3.1 for Windows, GraphPad Software, San Diego, California USA) was used to perform paired t-tests and one- and two-way repeated measures ANOVAs followed by Dunnett post-hoc tests; while Origin Pro 9 (OriginLab Corporation, Northampton, MA) was used to perform Mauchly's test of sphericity prior to ANOVA. Specifically, if Mauchly's test was significant ( $\chi^2$ , p-value, and  $\epsilon$  were reported in this case) and, thus, equal variance between pairs could not be assumed, then a repeated measures ANOVA with a Greenhouse-Geisser correction was performed with GraphPad Prism. *P*-values of less than 0.05 were considered statistically significant. All data are expressed as mean  $\pm$  SEM unless otherwise specified.

## 3. Results

### 3.1. LOT stimulation activated postsynaptic inhibitory granule cells preferentially

Electrical stimulation of mitral cell axons in LOT preferentially excites postsynaptic granule cells, the most common GABAergic neurons in the olfactory bulb, via reciprocal dendrodendritic synapses between the lateral dendrites of presynaptic mitral cells and the spines of postsynaptic granule cells in EPL (Fig. 1A) (Chen et al., 2000; Halabisky et al.,

2000; Isaacson and Strowbridge, 1998; Laaris et al., 2007; Schoppa et al., 1998). Dendrodendritic synapses of inhibitory periglomerular cells in GL can also be activated by LOT stimulation, but experimental evidence suggested that their contributions were negligibly small (Bardoni et al., 1996; Freeman, 1974; Laaris et al., 2007; Poplawsky et al., 2015; Wellis and Scott, 1990). In addition, the location of our stimulating electrode near Bregma was chosen to minimize the contributions of tufted cells that have largely terminated in more rostral brain regions (Igarashi et al., 2012). We confirmed this targeted activation by double immunostaining for c-Fos and GAD<sub>67</sub>. While c-Fos is expressed exclusively in the cell nucleus (Dragunow and Faull, 1989; Kovacs, 1998), GAD<sub>67</sub> stains the cytoplasm of GABAergic cells (Erlander et al., 1991; Esclapez et al., 1994). Hoechst stain for DNA was also used to confirm the location of nuclei for c-Fos imaging. C-Fos positive nuclei (green) were prominent in the mitral cell layer (MCL) and GCL, with few positive nuclei in EPL (Fig. 1B, one representative rat), which was consistent to an earlier report (Wilson et al., 1996). The presence of c-Fos staining in the nuclei of mitral cells in MCL (\*), without concomitant cytoplasmic GAD<sub>67</sub> staining, was due to the direct stimulation of their axons in LOT; similar to the few positive nuclei in EPL (>) that were presumably excitatory tufted cells. In addition, a large population of GAD<sub>67</sub> containing granule cells in GCL had c-Fos positive nuclei (<) for all four rats. These results support that postsynaptic inhibitory granule cells were indeed exclusively activated via dendrodendritic synapses by our LOT-stimulation paradigm.

Excitation of inhibitory granule cells can be further confirmed by electrophysiology. A single-pulse stimulation of LOT suppressed, presumably, mitral and tufted cells' spontaneous spiking activity in EPL (Fig. 1C top) (see also Fig. 4 in Wilson et al., 1996), similar to pulse-train stimulations (Fig. 1C bottom). LFPs recorded in GCL following LOT stimulation had the signature triphasic form (black line, Fig. 1D), whereby the first phase (1) was suspected to be the elicited antidromic spike, the second (2) to be depolarization of the granule cells, and the third (3) to be mediated by inhibition of mitral cells and/or other polysynaptic responses (Mori and Takagi, 1978; Nakashima et al., 1978; Nicoll, 1969; Rall and Shepherd, 1968; Uva et al., 2006). Suppression of the second LFP phase with a topical application of an NBQX and APV mixture, ionotropic AMPA and NMDA glutamate receptor antagonists, respectively, (red line) and its subsequent recovery with drug washout (blue line) confirmed its postsynaptic origin (Wilson et al., 1996).

The optimal stimulation frequency of LOT to evoke LDF responses under isoflurane was 40 Hz, the same as with  $\alpha$ -chloralose anesthesia (not shown). We then varied the current intensity to examine the relationship of the LFP and LDF response amplitudes evoked by LOT stimulation (Fig. 1E). The evoked response amplitudes increased with stimulation current intensity; both LFP and LDF responses were smallest at  $-50 \mu\text{A}$  and largest at  $-200 \mu\text{A}$  (Fig. 1E). To quantify the relationship between LFP and LDF amplitudes, we calculated the area under the LFP ( $\Sigma\text{LFP}$ ) and LDF ( $\Sigma\text{LDF}$ ) signals during the stimulation period for each stimulus current and normalized by their maxima. Stimulus current modulation showed an exponential relationship between the evoked blood flow responses and LFPs recorded in GCL (Fig. 1F,  $\text{LDF} = y_0 + Ae^{R_0\text{LFP}}$ ,  $y_0 = (8.61 \pm 27.39) \times 10^{-3}$ ,  $A = (4.65 \pm 4.93) \times 10^{-4}$ ,  $R_0 = 7.67 \pm 1.05$ ,  $R^2 = 0.96$ ), indicating that a small decrease in the LFP amplitude caused a

large decrease in the amplitude of the blood flow response. We, therefore, largely confirmed that the postsynaptic cells activated by LOT stimulation were exclusively GABAergic that then, in turn, reciprocally suppressed mitral cell activity.

### 3.2. Blockade of postsynaptic granule cell activity decreased CBVw-fMRI responses to LOT stimulation

Our previous CBVw-fMRI studies using the same rat olfactory bulb model showed layer-specific blood volume increases in EPL during LOT stimulation (Poplawsky et al., 2015). Here, we topically applied 25-mM APV, an NMDA receptor antagonist, for 90 min to pharmacologically block the postsynaptic responses of inhibitory granule cells evoked by LOT stimulation (64 s duration, ~5-min interstimulus interval). Fig. 2A shows an image of the cranial window with an acrylic coverslip and inlet and outlet tubes for remote topical drug delivery. T2-weighted anatomical images of the bulb showed the location of the vehicle or drug (blue overlay) and where it interfaced with the bulb surface (Fig. 2B, red arrows). During the 60-min vehicle control period, evoked responses to LOT stimulation had a typical pattern with the strongest activation in middle layers, including EPL (Fig. 2C top, representative rat,  $p < 0.01$  voxel- and family-wise error correction with a minimum of 22 voxels in a cluster), as previously reported (Poplawsky et al., 2015). The proportion of activated-to-total voxels in noise regions outside of the brain (i.e., estimate of type-1 error) was  $< 1\%$  for the control condition of all rats. Furthermore, the contralateral bulb served as an internal control since LOT stimulation primarily evoked large increased CBVw responses in the ipsilateral bulb due to its unilateral projections. Some activations were observed at the bulb midline that was likely residual nonspecific activation from the large midline vessels or fMRI signal spread. When these activations were ignored, the proportion of activated-to-total voxels in the contralateral bulb was  $< 1\%$ . Interestingly, all activated voxels in the contralateral bulb of one rat had decreased CBV, consistent with our previous study (Poplawsky et al., 2015), suggesting this to be true activation. Therefore, the thresholding method chosen adequately controlled for type-1 error. When APV was applied on the dorsal surface, CBVw-fMRI responses decreased near the site of application (Fig. 2C middle), while fMRI responses remained intact in the regions farther away. During the 180-min drug washout period, the evoked responses in the impacted regions mostly returned to the pre-drug control levels with some exceptions to regions nearest to the drug application site (Fig. 2C bottom).

Next, we cross-referenced the above-threshold evoked responses to LOT stimulation during the control period (Fig. 2D left,  $p < 0.01$  voxel- and family-wise error corrected) with the distance from the APV application site identified with anatomical MRI (Fig. 2D middle) to quantify the distance-dependency of the CBVw-fMRI responses to APV (Fig. 2D right). We then obtained fMRI time courses from bins of increasing distance (Fig. 2E, 9 slices per rat,  $n = 5$  rats). Time-dependent signals decreased with APV (red lines) most significantly at sites nearest to the application site, with nearly negligible effects farther than 1.5 mm. Mean percent signal changes due to LOT stimulation from these same voxels were statistically tested using a one-way repeated measures ANOVA to examine the effects of APV at each binned distance. In this study, recovery of LOT-stimulation evoked responses was defined by the significant reversal of drug-induced effects rather than complete recovery to pre-drug

baseline levels because complete washout of the drugs was not expected (for details, see the Discussion). Therefore, Dunnett's post-hoc tests were used to compare the drug period to the pre-drug control and washout periods only (see Methods). Evoked fMRI responses during stimulation significantly decreased due to APV at 0–1.5 mm from the drug application site (Fig. 2F): 0–0.5 mm ( $-50.36 \pm 13.06\%$ ,  $F(2, 8) = 7.565$ ,  $p = 0.014$ ; Control vs. APV,  $p = 0.010$ ), 0.5–1.0 mm ( $-46.46 \pm 5.68\%$ ,  $F(2, 8) = 19.951$ ,  $p < 0.001$ ; Control vs. APV,  $p < 0.001$ ), 1.0–1.5 mm ( $-29.37 \pm 5.22\%$ ,  $F(2, 8) = 7.643$ ,  $p = 0.014$ ; Control vs. APV,  $p = 0.012$ ). While evoked fMRI responses did not significantly recover at the most superficial 0–0.5 mm distance (APV vs. Washout,  $p = 0.524$ ), they did significantly recover at the 0.5–1.5 mm distances (APV vs. Washout, 0.5–1.0 mm:  $p = 0.013$ ; 1.0–1.5 mm:  $p = 0.029$ ). No significant effects of APV were measured beyond 1.5 mm from the drug application site (1.5–2.0 mm,  $F(2, 8) = 3.531$ ,  $p = 0.080$ ; 2.0–2.5 mm,  $F(2, 8) = 2.179$ ,  $p = 0.176$ ;  $> 2.5$  mm,  $F(2, 8) = 0.842$ ,  $p = 0.466$ ).

To further examine the APV effective area in higher spatial detail, we calculated voxel-wise maps of the drug-induced changes in the evoked fMRI responses using a linear regression analysis. Only voxels that had significant responses during the pre-drug control period (primary GLM,  $p < 0.01$  voxel- and family-wise error corrected) were included in the analysis and only significant voxels in the spatial maps of APV effects ( $p < 0.05$  voxel- and family-wise error correction with a minimum of 79 voxels in a cluster) were evaluated. The resultant percent change maps had decreased evoked fMRI responses (i.e., blue-colored deactivations) due to APV, which had localized effects at the drug application site (Fig. 3, A and B, two representative rats). We did not calculate any significant deactivation for Rat 3, although some subthreshold deactivation was noted (see also Fig. 2F, filled circles). Also, a diminished number of significant voxels was sometimes observed in the dorsal bulb nearest to the drug application site that was likely due to these regions not recovering completely from the APV washout, which is a condition of this analysis (compare also Fig. 2C and 3A second slice from left, both from Rat 2). It is noted that no deactivations were observed in noise regions outside of the bulb or beyond 2.5 mm from the drug application site for all rats, which confirmed adequate control of type-1 error. We further examined the temporal dynamics (~5-min resolution) of the drug effects by averaging the percent fMRI signal changes to each LOT stimulation for all deactivated voxels. The mean deactivation (Fig. 3C, black line,  $n = 4$  rats) was greatest ~30 min after APV application (gray bar) and recovered another ~30 min following drug washout. In all, the maximum suppression effects of APV occurred up to 1.5 mm below the drug application site within 30 min.

### 3.3. Blockade of postsynaptic granule cell activity decreased the blood flow responses to LOT stimulation

The above results suggest that the CBVw-fMRI response evoked by LOT stimulation is mediated by the postsynaptic activity of inhibitory granule cells. Although CBVw fMRI was used to examine the depth-dependent effects of APV, it was necessary to directly compare the neurophysiological and hemodynamic changes caused by the drug using non-MRI techniques. First, we recorded blood volume increases to LOT stimulation by OIS imaging at the 572-nm isosbestic point of hemoglobin (Fig. 4A – C,  $n = 1$  rat) for direct comparison to our CBVw-fMRI results, in addition to concurrent blood flow measurements using a

single LDF probe. LOT stimulation caused darkening (i.e., increased light absorption or decreased light reflection) on the dorsal surface of the bulb (Fig. 4, A and B), indicative of increased blood volume. The amplitudes of the blood volume responses were somewhat varied depending on the location, but the temporal patterns consistently had two peaks with an initial fast response followed by a slower one (Fig. 4C). Although these OIS measurements from the bulb surface were comparable to our CBVw-fMRI measurements in EPL (Fig. 2E, see also Fig. 8 in Poplawsky et al., 2015), noteworthy differences included a more prominent initial peak and a plateauing of the subsequent slower response before the stimulus offset for the OIS data. In addition, the time courses of optical blood flow and blood volume measurements were similar, except for a small sustained post-stimulus response in the blood volume signal compared to the flow (Fig. 4D). Due to the relative consistency of both optical measurements and the homogeneity of the signal changes independent of the measurement location, we chose a single point LDF measurement to reflect blood flow and volume changes in the dorsal olfactory bulb for the remainder of our study.

Concurrent electrophysiological recordings in GCL (Fig. 4E, top,  $n = 8$  rats) and LDF at the bulb surface (Fig. 4F, top) showed that a train of stimulation pulses in LOT evoked LFPs and concomitant blood flow increases in the bulb, respectively, during the pre-drug control period (black traces). Note, LFP envelopes are shown instead of raw LFPs (inset in Fig. 4E) hereafter for ease of comparison. Using an electrical stimulation of 40 Hz, each stimulation pulse evoked a triphasic LFP response with negligible amplitude attenuations over 64 s. Topical application of APV decreased LFP amplitudes and blood flow responses (red traces); both of which recovered after washout of the drug (blue traces). To further quantify the changes in the evoked responses due to APV, we calculated the area under the LFP ( $\Sigma$ LFP) and LDF ( $\Sigma$  LDF) signals during the stimulation period for the pre-drug control, APV-applied, and washout periods, respectively. For  $\Sigma$ LFP, Mauchly's test of sphericity was significant ( $\chi^2(2) = 6.290$ ,  $p = 0.043$ ), thus equal variance was not assumed. As such, one-way repeated measures ANOVA with a Greenhouse-Geisser correction ( $\epsilon = 0.606$ ) was conducted and a significant difference was determined ( $F(1.213, 8.488) = 9.707$ ,  $p = 0.011$ ).  $\Sigma$ LFP significantly decreased by  $43.82 \pm 15.47\%$  with APV (Fig. 4E bottom; Control vs. APV,  $p = 0.044$ ). Compared to the LFP responses, APV effects on the LDF responses were much stronger:  $\Sigma$  LDF significantly decreased by  $84.59 \pm 2.63\%$  (Fig. 4F bottom; one-way repeated measures ANOVA,  $F(2,14) = 23.117$ ,  $p < 0.001$ ; Control vs. APV,  $p < 0.001$ ). After washout of the drug, both LFP (APV vs. Washout,  $p = 0.004$ ) and LDF (APV vs. Washout,  $p = 0.007$ ) responses recovered. Spontaneous LFP signals had a significant drug effect (two-way repeated measures ANOVA, main APV effect,  $F(2,14) = 17.894$ ,  $p < 0.001$ , not shown). Only the gamma-band was further examined since this frequency correlates well with hemodynamic responses (Logothetis et al., 2001; Nielsen and Lauritzen, 2001; Viswanathan and Freeman, 2007), which significantly decreased by  $8.5 \pm 1.8\%$  (Control vs. APV,  $p < 0.001$ ) and recovered (APV vs. Washout,  $p < 0.001$ ). Interestingly, baseline LDF signals remained unchanged (one-way repeated measures ANOVA,  $F(2,14) = 0.837$ ,  $p = 0.454$ , not shown), suggesting that these baseline neuronal activity changes likely did not largely affect blood flow. Since the effects of APV were similar between CBVw fMRI (Figs. 2 and 3) and LDF (Fig. 4), we used LDF as a surrogate measure of CBVw fMRI in the following

experiments to allow for measurements of regional blood flow and simultaneous electrophysiology during a higher throughput pharmacological examination.

We next repeated this pharmacological study with NBQX, an AMPA receptor antagonist, in a separate group of rats (Fig. 4, G and H,  $n = 6$  rats). Unlike blocking NMDA receptors, blocking AMPA receptors decreased neuronal and blood flow responses almost equally: NBQX significantly decreased postsynaptic activities of granule cells by  $83.96 \pm 1.49\%$  (Fig. 4G; one-way repeated measures ANOVA with a Greenhouse-Geisser correction (Mauchly's test,  $\chi^2(2) = 6.272$ ,  $p = 0.043$ ,  $\epsilon = 0.558$ ),  $F(1.116, 5.582) = 41.568$ ,  $p < 0.001$ ; Control vs. NBQX,  $p = 0.002$ ) and blood flow responses by  $80.71 \pm 5.28\%$  (Fig. 4H; one-way repeated measures ANOVA with a Greenhouse-Geisser correction (Mauchly's test,  $\chi^2(2) = 9.852$ ,  $p = 0.007$ ,  $\epsilon = 0.522$ ),  $F(1.044, 5.222) = 9.327$ ,  $p = 0.026$ ; Control vs. NBQX,  $p = 0.032$ ) compared to the control period. After drug washout, LFP (NBQX vs. Washout,  $p = 0.003$ ) and LDF responses (NBQX vs. Washout,  $p = 0.005$ ) significantly recovered. Similar to APV, NBQX decreased the baseline neuronal activities (two-way repeated measures ANOVA, main NBQX effect was Greenhouse-Geisser corrected (Mauchly's test,  $\chi^2(2) = 7.655$ ,  $p = 0.022$ ,  $\epsilon = 0.540$ ),  $F(1.080, 5.398) = 8.668$ ,  $p = 0.028$ , not shown), and specifically decreased the gamma-band LFP power by  $10.2 \pm 2.4\%$  (Control vs. NBQX,  $p = 0.015$ ; NBQX vs. Washout,  $p = 0.026$ ). However, the baseline LDF signals did not change ( $F(2, 10) = 3.670$ ,  $p = 0.064$ , not shown). To further examine whether the vasculature directly reacted with the antagonists, a mixture of 5-mM NBQX and 25-mM APV was applied on the right bulb only while blood flow was measured in both the left and right bulbs. During a ~4% hypercapnic challenge, the blood flow increased similarly in both bulbs (not shown), which confirmed that the vascular reactivity was unchanged by the drugs. Collectively, these results suggest that postsynaptic activities, namely NMDA- and AMPA-derived depolarizations, of inhibitory granule cells contribute to the evoked hemodynamic responses.

### 3.4. Blockade of astrocytic glutamate transporters did not suppress the blood flow responses to LOT stimulation

The above results support that the excitation of postsynaptic inhibitory granule cells was responsible for the evoked hemodynamic responses. However, the NBQX and APV glutamate receptor antagonists could also modulate astrocytic activity by inhibiting their glutamate reuptake (Lalo et al., 2006), and, thus, these antagonists may have interfered with astrocytic hemodynamic regulation (Gurden et al., 2006; Petzold et al., 2008). Astrocyte glutamate transporters, like GLAST and GLT-1, are responsible for the bulk reuptake of extracellular glutamate in the bulb (Utsumi et al., 2001). To determine whether presynaptic glutamate release can also increase blood flow through astrocytes, we applied 1-mM DHK on the dorsal surface of the bulb ( $n = 7$  rats) to inhibit the astrocyte-specific glutamate transporter, GLT-1. DHK increased baseline neuronal activities (Fig. 5A, two-way repeated measures ANOVA, main DHK effect,  $F(1, 6) = 27.199$ ,  $p = 0.002$ ), specifically the baseline gamma-band power increased by  $2.86 \pm 0.43\%$ , which we examined with a paired  $t$ -test since a washout period was not performed (Control vs. DHK,  $p < 0.001$ ,  $n = 7$  rats). In addition, baseline LDF signals increased by  $15.08 \pm 4.17\%$  (Fig. 5B, paired  $t$ -test,  $p = 0.015$ ). Baseline LFP, and subsequently LDF, signals likely increased due to impaired glutamate buffering. Conversely, for LOT stimulation, we observed a small  $4.29 \pm 1.97\%$

decrease in the LFP signals (Fig. 5C, paired *t*-test,  $p < 0.001$ ) corresponding to a  $24.15 \pm 9.76\%$  increase in the concomitant blood flow response (Fig. 5D, paired *t*-test,  $p = 0.039$ ) due to DHK. DL-threo- $\beta$ -Benzyloxyaspartic acid (TBOA), which can inhibit both GLAST and GLT-1, was not used because it depolarizes mitral cells (De Saint Jan and Westbrook, 2005; Vincis et al., 2015) and changes the basal state of the neurovascular network (Otsu et al., 2015). However, DHK may have similar problems since it was unexpected that evoked blood flow responses would increase with subtle decreases in LFP, possibly caused by impaired glutamate buffering itself. Nonetheless, evoked blood flow responses did not decrease, suggesting that astrocytes are not mediating the evoked blood flow responses to LOT stimulation through glutamate transporters.

This finding contradicts previous reports that pharmacological blockade of glutamate transporters using TBOA decreased hemodynamic responses to odor stimulation in the bulb (Gurden et al., 2006; Petzold et al., 2008; but see, Vincis et al., 2015). To verify the effects of DHK on the blood flow responses evoked by odor stimulation, we stimulated the rat with a strong dorsal bulb activating odor, 0.8% 2-hydroxyacetophenone in mineral oil, and found that blood flow responses were not changed significantly by DHK (Control vs. DHK for  $\Sigma$  LDF:  $14.16 \pm 4.92\%$  vs.  $20.78 \pm 3.24\%$ ,  $p = 0.161$ ,  $n = 7$  rats). Although the reason for this discrepancy is unclear, it may be related to differential changes in the basal state of the circuit caused by each drug (De Saint Jan and Westbrook, 2005; Otsu et al., 2015; Vincis et al., 2015).

### 3.5. Inhibition of nitric oxide synthase preferentially decreased the initial, fast component of the blood flow responses to LOT stimulation

We next investigated the role of nitric oxide (NO) to the hemodynamic response caused by increased inhibitory granule cell activity. NO was shown to mediate vessel dilation following increased neuronal activity in the neocortex and cerebellum (Echagarruga et al., 2020; Rancillac et al., 2006). We applied 1-mM L-NNA, a nonspecific NOS inhibitor, to the bulb and measured the blood flow and electrophysiological changes. L-NNA is an irreversible antagonist without L-arginine (Mayer et al., 1993), so a washout period was not performed. L-NNA did not change baseline neuronal activity, including baseline gamma-band power (Fig. 6A, two-way repeated measures ANOVA, main L-NNA effect,  $F(1,6) = 0.649$ ,  $p = 0.451$ ,  $n = 7$  rats), while it decreased baseline LDF signals by  $23.52 \pm 5.40\%$  (Fig. 6B, paired *t*-test, Control vs. L-NNA,  $p = 0.004$ ), presumably due to vasoconstriction induced by the inhibition of baseline NO release. The mean evoked LFP (Fig. 6C) and LDF (Fig. 6D) responses also decreased with L-NNA application. However, the fast, initial blood flow response appeared to be preferentially inhibited compared to the second, slower phase; thus, we analyzed them separately. The evoked LFP responses decreased similarly for the initial (Fig. 6E top, 0 – 10 s, paired *t*-test,  $11.09 \pm 1.86\%$ ,  $p = 0.001$ ) and later (Fig. 6E bottom 10 – 64 s,  $11.01 \pm 1.99\%$ , paired *t*-test,  $p = 0.002$ ) phases. Conversely, the initial LDF response decreased by  $47.17 \pm 10.18\%$  (Fig. 6F top, 0 – 10 s, paired *t*-test,  $p = 0.008$ ), while the later phase decreased by  $19.54 \pm 12.20\%$  although it did not reach statistical significance (Fig. 6F bottom, 10 – 64 s, paired *t*-test,  $p = 0.301$ ). Therefore, NO signaling may be contributing more to the initial, fast neurovascular response compared to the later, sustained response.

### 3.6. Blockade of vasoactive intestinal peptide receptors did not suppress the blood flow responses to LOT stimulation

Neuropeptides are often co-released with GABA. Among them, vasoactive intestinal peptide (VIP) was found to dilate vessels in slice preparations (Cauli et al., 2004). Therefore, we applied a VIP receptor antagonist, VIP (6–28), to the bulb surface and tested whether it altered blood flow responses. A 0.1-mM VIP (6–28) solution did not change baseline neuronal activity, including baseline gamma-band power (two-way repeated measures ANOVA, main VIP (6–28) effect,  $F(1,5) = 1.555$ ,  $p = 0.268$ ,  $n = 6$  rats, not shown), and baseline LDF signals (paired  $t$ -test, Control vs. VIP (6–28),  $p = 0.174$ , not shown). Similarly, the antagonist had no significant effect on evoked LFPs (Fig. 7A, paired  $t$ -test,  $p = 0.092$ ) or blood flow responses (Fig. 7B, paired  $t$ -test,  $p = 0.686$ ) compared to the control period.

### 3.7. Blockade of presynaptic GABA release decreased blood flow responses to LOT stimulation

Lastly, we examined the effects of GABA on the hemodynamic response to LOT stimulation by applying 10-mM baclofen, a GABA<sub>B</sub> autoreceptor agonist, to suppress granule cell GABA release. While baclofen strongly inhibited GABA release from granule cell spines, it also mildly inhibited glutamate release from the lateral dendrites of mitral cells (Isaacson and Vitten, 2003). Therefore, a slight reduction of evoked LFPs by LOT stimulation was expected with baclofen application. Indeed, baclofen reduced the LFP responses by  $16.73 \pm 2.36\%$  (Fig. 7C, one-way repeated measures ANOVA,  $F(2,16) = 44.566$ ,  $p < 0.001$ ; Control vs. Baclofen,  $p < 0.001$ ,  $n = 9$  rats) and LDF responses by  $55.28 \pm 7.23\%$  (Fig. 7D, one-way repeated measures ANOVA,  $F(2,16) = 30.244$ ,  $p < 0.001$ ; Control vs. Baclofen,  $p < 0.001$ ). However, the evoked LFP (Baclofen vs. Washout,  $p = 0.166$ ) and LDF responses (Baclofen vs. Washout,  $p = 0.755$ ) did not recover with washout; although they appeared to stabilize rather than decrease further (see Discussion). Baclofen application also changed baseline neuronal activity (two-way repeated measures ANOVA, main baclofen effect was Greenhouse-Geisser corrected (Mauchly's test,  $\chi^2(2) = 9.815$ ,  $p = 0.007$ ,  $\epsilon = 0.570$ ),  $F(1.140, 9.122) = 13.203$ ,  $p = 0.004$ , not shown), specifically the gamma-band decreased by  $5.90 \pm 1.89\%$  (Control vs. Baclofen,  $p = 0.019$ ), that did not recover with drug washout (Baclofen vs. Washout,  $p = 0.961$ ). Baseline LDF signals did not change (one-way repeated measures ANOVA,  $F(2,16) = 0.106$ ,  $p = 0.900$ , not shown). Nonetheless, response decreases with baclofen possibly indicates that GABA release is necessary for the hemodynamic response to LOT stimulation, although a concomitant decrease in GABAergic postsynaptic activity is a plausible alternative.

## 4. Discussion

We examined the role of inhibitory neurons to neurovascular coupling using the same layer-specific rat olfactory bulb model that we previously described, whereby elicited hemodynamic responses were confined to EPL (Poplawsky et al., 2019a, 2015). In the present study, we confirmed that stimulation of LOT preferentially activated inhibitory granule cells through dendrodendritic synapses (Fig. 1). During simultaneous fMRI and topical pharmacology, we found localized (up to 1.5 mm below the bulb surface) decreases in the CBVw-fMRI responses to LOT stimulation with postsynaptic blockade of granule cell

NMDA receptors, which recovered following drug washout (Figs. 2 and 3). We independently replicated these findings without fMRI to show concomitant LDF blood flow and LFP decreases to NMDA and AMPA receptor antagonists (Fig. 4), supporting that postsynaptic activation of inhibitory granule cells is necessary for the observed functional hyperemia. Interestingly, blockade of GABA release from granule cells significantly decreased blood flow, although a similar LFP decrease was also observed (Fig. 7, C and D). We further determined that glutamate reuptake by astrocytes (Fig. 5), NO (Fig. 6), and VIP (Fig. 7, A and B) did not contribute considerably to the evoked hemodynamic responses, particularly to the slower portion, despite a putative presence of GABAergic cells in rat EPL containing VIP (Gall et al., 1986; Miller et al., 2014). We did observe, however, a relatively larger contribution of NO to the initial, fast blood flow response compared to the later phase.

#### 4.1. Role of astrocytes in neurovascular coupling of inhibitory neurons

Neurovascular coupling has been extensively examined in the olfactory bulb glomerular model. In contrast to our LOT-stimulation model, previous studies postsynaptically activated both excitatory mitral cells and inhibitory periglomerular cells, thus, making it difficult to assess the contributions of each neuron type to the hemodynamic response. In addition, conclusions from the glomerular model were controversial on whether neurovascular coupling was initiated by presynaptic glutamate detection by astrocytes (Gurden et al., 2006; Petzold et al., 2008) or by astrocytic activity initiated by the postsynaptic neuron (Otsu et al., 2015). Because our results support hemodynamic responses initiated by postsynaptic activity of inhibitory neurons (Figs. 2–4) and not by astrocyte glutamate reuptake (Fig. 5), we further tested whether astrocyte involvement could be unique to the glomerular model using our experimental procedures. Therefore, we examined the effects of DHK on blood flow responses to a relatively strong odor stimulation (~0.8% w/w), but did not find a significant effect. Some of the disparity between astrocytic and neuronal postsynaptic mechanisms could be accounted for by non-hemodynamic contributions to the OIS signal (Vincis et al., 2015), indirect changes in neuronal activity caused by an astrocyte glutamate transporter blocker, such as TBOA (De Saint Jan and Westbrook, 2005; Otsu et al., 2015; Vincis et al., 2015), absence of astrocyte mGluR5 in adult rodents (Sun et al., 2013), or stimulus-specific activation of single vs. multiple neighboring glomeruli (Chaigneau et al., 2007; Jukovskaya et al., 2011; Petzold et al., 2008). Furthermore, delayed and prolonged hemodynamic responses were not predicted well by neuronal activity (Aydin et al., 2020) but by astrocytic activity (Schulz et al., 2012); thus, we cannot rule out astrocyte involvement through secondary mechanisms independent of glutamate detection, such as potassium buffering (Filosa et al., 2006; Girouard et al., 2010; Witthoft et al., 2013) or ATP detection (Mishra et al., 2016; Wells et al., 2015), both of which depend on postsynaptic activity. Alternatively, our gradual rise-to-peak responses (e.g., Fig. 2E) may be related to the slow and long-lasting kinetics of dendrodendritic inhibition, which depends on NMDA receptor activation on granule cells (Isaacson and Strowbridge, 1998; Schoppa et al., 1998). Clearly, more studies are needed to determine whether neurovascular coupling mechanisms of excitatory and inhibitory neurons are different, and whether astrocytes play a role.

#### 4.2. Role of NOS in neurovascular coupling of inhibitory neurons

NOS inhibition had a stronger effect on the initial, fast blood flow response compared to the later, sustained phase. NOS positive staining is primarily found in periglomerular and granule cell bodies in GL and GCL, respectively, as well as other sparsely-stained inhibitory interneurons with cell bodies in EPL and GCL (Kishimoto et al., 1993; Kosaka and Kosaka, 2007; Spessert et al., 1994; Weruaga et al., 2000). This matches well with the laminar distribution of tonic NO production imaged in olfactory bulb slices, with the highest NO signals found in GL and GCL that were weaker in EPL (McQuade et al., 2010). Although periglomerular cells are not activated much by LOT stimulation (Bardoni et al., 1996; Freeman, 1974; Wellis and Scott, 1990), NOS containing granule cells are expected to be evoked. But, it is unknown whether their apical dendrites contain NOS or whether NO is released by activated granule cell spines in EPL through comparable functional coupling of NOS to the NMDA receptor signaling complex observed else-where (Aoki et al., 1997; Hardingham et al., 2013; Husi et al., 2000). Similar to our observations, NOS inhibitors only slightly affected hemodynamic responses evoked by somatosensory stimulation (Lecrux et al., 2011; Vazquez et al., 2018) (but see, Stefanovic et al., 2007), although direct activation of NOS neurons in the primary somatosensory cortex evoked vasodilation (Krawchuk et al., 2020; Lee et al., 2020b). Nonetheless, since the initial CBF and CBVw fMRI responses are less specific to the evoked layer compared to later components (Jin and Kim, 2008), our data suggest that NOS may control transient penetrating arteriole dilation. It is noted that other vascular pathways cannot be ruled out since L-NNA inhibits both neuronal and endothelial NOS. Considering the diversity of GABAergic interneurons and the incomplete effect of NOS blockade on functional hyperemia in the current study, it is not surprising that other neurovascular signaling pathways exist (Hosford and Gourine, 2019) independent of NO signaling.

#### 4.3. Considerations for the recovery from drug effects

Response recovery following drug washout is complex and is dependent on the experimental procedures and the chemical properties of the drug (see Methods section). For baclofen, both neuronal activity and blood flow responses did not significantly recover with washout, yet both responses also remained steady between drug and washout periods (Fig. 7, C and D). Furthermore, the fMRI measurements (Fig. 2E and F) consistently showed that the amplitude of drug effect was maximal at the drug application site and lessened with increasing distance; and that fMRI response recovery with washout was poorest at the drug application site and improved at intermediate distances (~0.5–1.5 mm). Therefore, recording at the surface, where the LDF measurements were biased, was optimized for detecting drug induced decreases in blood flow but not recovery. Finally, the CBVw-fMRI responses in regions distal to the drug application site did not differ much between the three conditions (Fig. 2, E and F, > 2.5 mm columns), suggesting that nonspecific procedural confounds (e.g., repeated LOT stimulation, duration of anesthesia, etc.) did not contribute much to the response decreases during drug application. Together, these support that the response changes with drug application were specific to the drug effects and that, likely, the drug was still acting in EPL during the washout period when responses did not completely recover.

#### 4.4. Time course differences between CBVw-fMRI and LDF responses

Time-dependent hemodynamic responses evoked by LOT stimulation were similar between LDF (Fig. 4F) and CBVw-fMRI measurements (Fig. 2E, 0–0.5 mm); thus, LDF was a good approximation for fMRI. However, for fMRI measurements, the initial peak was less distinct, and the second phase had a slower rise-time and later peak compared to LDF. These observations likely reflected differences in the vascular compartments that each technique was more sensitive to. Specifically, LDF measurements can be biased toward upstream vessels above EPL, including larger, nonspecific pial vessels; although it is also sensitive to changes within EPL since most of the signal comes from 0 to 0.5 mm below the brain surface (Fredriksson et al., 2009). Conversely, CBVw-fMRI measurements are less sensitive to these larger vessels due to increased magnetic susceptibilities and baseline signal dropouts caused by MION (Kennan et al., 1998; Mandeville et al., 1998; Poplawsky and Kim, 2014; van Bruggen et al., 1998). Furthermore, fMRI responses evoked by LOT stimulation can be biased toward smaller, local vessels that dilate approximately 100  $\mu\text{m}$  beyond the evoked synapses in EPL (Poplawsky et al., 2019a). It is controversial whether capillaries near the synapse dilate considerably (Rungta et al., 2018), although fMRI may be sensitive to even small dilations because it integrates changes over the entire vessel population within the voxel. Interestingly, the temporal profile of the LDF signal during baclofen application (Fig. 7D red line) was similar to the fMRI time courses (Fig. 2E), especially when comparing the slow, prolonged rise of the second signal phase. It is intriguing to speculate whether GABA release in EPL can trigger vascular backpropagation to nonspecific surface vessels (Chen et al., 2014; Iadecola et al., 1997; Longden et al., 2017; Tian et al., 2010) without affecting local vessels.

#### 4.5. Synaptic vs. optogenetic activation of inhibitory neurons

In the current study, we examined the contributions of synaptically driven inhibitory neurons to the hemodynamic response, which is in contrast to studies that elicited inhibitory neuronal activity through ChR2 (Anenberg et al., 2015; Uhlirva et al., 2016; Vazquez et al., 2018), a genetically-modified nonselective cation channel gated by light. Although both results show that activation of inhibitory neurons increases hemodynamic responses, synaptic activation is important because our results and previous studies imply that hemodynamic responses were mediated by calcium entry, since blocking postsynaptic NMDA receptors impaired sensory-stimulation evoked hemodynamic responses as much as blocking AMPA receptors (Gsell et al., 2006; Nielsen and Lauritzen, 2001). Therefore, the permeability of ChR2 to calcium (Nagel et al., 2003) can bypass NMDA receptor-dependent calcium signaling or change the relationship between the synaptically evoked LFP and the hemodynamic response (Iordanova et al., 2015). Second, our previous fMRI results in the olfactory bulb showed that the location of blood volume increases was specific to the active synapse. Particularly, we observed peak CBVw-fMRI changes at the distal synapses in EPL and at the proximal synapses in GCL of the same inhibitory granule cells when these precise synapses were independently targeted with LOT and anterior commissure stimulations, respectively (Poplawsky et al., 2019b, 2015). This indicated that neurovascular signaling units are compartmentalized, possibly within the dendritic spines or equivalent microdomains, that may not transmit over the entire neuron. Currently, ChR2 is distributed throughout the neuronal membrane and is not specific to the synapse, which may initiate other nonspecific,

calcium-dependent processes that confound synaptic neurovascular coupling. Nonetheless, targeted stimulation of inhibitory neurons by both synaptic activation and ChR2 can initiate hemodynamic responses, independently validating the role of these neurons in neurovascular coupling.

#### 4.6. Generalizations to characteristic neurovascular coupling

The cytoarchitecture and function of the olfactory bulb (Nagayama et al., 2014) differ from other sensory cortices and raises the concern of whether these results are generalizable to the neocortex. Namely, there are more GABAergic than excitatory neurons in the bulb (Lledo et al., 2008) and synaptic transmission often occurs through reciprocal dendrodendritic synapses (Schoppa et al., 1998), which we retrogradely activated. The vascular topography of the bulb also has some contrasting features compared to the primary somatosensory cortex (Blinder et al., 2013; Lecoq et al., 2009; Poplawsky et al., 2019a). Despite these differences, the metabolic regulation of blood flow seems consistent between the bulb and other sensory cortices, whereby the microvascular density parallels the cytochrome oxidase activity across layers (Borowsky and Collins, 1989; Weber et al., 2008) and baseline  $P_{O_2}$  levels of microvessels in GL are similar to those in somatosensory cortical layers (Lyons et al., 2016). The anatomically specialized features of dendrodendritic synapses also have many similar functional aspects as axodendritic and axosomatic synapses of the neocortex with regards to synaptic transmission (see Schoppa et al. (1998) for a related discussion). Therefore, neurovascular principles are likely maintained between the bulb and other sensory cortices, although variations in metabolic and vascular dynamics should be considered between functionally distinct brain regions with unique cellular compositions.

Our LOT stimulation, and those of other optogenetic studies, evoke a more energetic state in the inhibitory neurons compared to peripheral stimulation. For instance, cytochrome oxidase activity is smallest in GCL, where the granule cell bodies reside, suggesting that inhibitory neurons are metabolically more efficient in their natural state. This is consistent to the observation that the smallest BOLD and CBVw fMRI responses evoked by odor stimulation is in GCL (Li et al., 2014; Poplawsky et al., 2015), despite having the largest gamma-band LFP responses (Li et al., 2014). Further, estimates of oxygen metabolism for inhibitory neurons in the primary somatosensory cortex suggests they have a relatively small impact on the overall tissue metabolic load (Vazquez et al., 2018). To clarify this issue, an oxygen consumption study is needed to examine how inhibitory neurons couple to the vasculature at varying metabolic levels.

#### 4.7. Assessment of circuit and vascular dynamic changes due to pharmacology

The association between LDF and LFP measurements to LOT stimulation for each drug is shown in Fig. 8. Here, most agents had a significant effect on the evoked LFPs validating that these drugs diffused through the dura mater. The only exception, VIP(6–28), was not expected to change neuronal activity (Lecrux et al., 2011), but ineffective penetration is possible due to its high molecular weight. Although the primary purpose of Fig. 8 was to summarize the results, we observed an exponential relationship similar to the stimulus-amplitude curve (Fig. 1F). This cautions us that pharmacological alteration of in vivo neural network dynamics can cause parallel hemodynamic changes, even if the specific pathway

tested has no direct role in neurovascular coupling. In particular, we observed blood flow decreases to baclofen, a presynaptic GABA-release blocker, suggesting that GABA may initiate functional hyperemia by astrocytic GABA reuptake (Doengi et al., 2009). Alternatively, manipulation of the excitatory-inhibitory balance by baclofen may have indirectly decreased the evoked LFPs and, subsequently, reduced hemodynamic responses. Therefore, caution should be used when considering the role of GABA release to neurovascular coupling from the current results. As this pertains to our main conclusion, we do not believe that network dynamic changes caused by indirect effects of the NMDA and AMPA receptor antagonists could cause the large decreases in the evoked hemodynamic responses. Specifically, we relied on a relatively simple neural circuit where a single population of inhibitory neurons was preferentially and directly targeted by LOT stimulation (Bartel et al., 2015; Laaris et al., 2007). Additionally, the evoked dendrodendritic synapses reciprocally inhibit the mitral cells, which limit the spatial extent for excitatory propagation to other synapses (Xiong and Chen, 2002). Therefore, these antagonists were preferentially acting at the first relay of a relatively isolated circuit, while glutamate release was preserved or enhanced by presynaptic disinhibition.

Interestingly, the AMPA receptor antagonist caused a twofold  $\Sigma$ LFP decrease compared to the NMDA receptor antagonist, while the  $\Sigma$  LDF decreases were similar. The larger  $\Sigma$ LFP decrease by the AMPA receptor antagonist indicates that NMDA receptors were likely also inhibited by this drug, since the release of magnesium blocks on NMDA receptors is facilitated by AMPA receptor activity (Chen et al., 2000). As for the similar  $\Sigma$  LDF decreases, this may be due to the slow-rise stage of the exponential relationship; or could indicate a calcium dependency for hemodynamic coupling (Lauritzen, 2005) since NMDA, and not AMPA, receptors mediate intracellular calcium increases (Chen et al., 2000; Halabisky et al., 2000; Isaacson and Strowbridge, 1998; Schoppa et al., 1998). In other words, the additional depolarization of granule cells by AMPA receptors may not contribute much to these hemodynamic responses due to their lesser association with calcium signaling. It is important to note that APV may act directly on NMDA receptors located on endothelial cells to inhibit functional hyperemia (Hogan-Cann et al., 2019; Lu et al., 2019), although we did not observe significant baseline LDF changes with the antagonist.

## 5. Conclusions

We conclude that postsynaptic activation of inhibitory granule cells, and not presynaptic action potentials or glutamate release alone, is necessary to elicit the hemodynamic response to LOT stimulation; and that NOS may be involved in the initial, but transient, vascular responses. Specifically, calcium influx associated with activation of granule cell NMDA receptors may underlie the synapse-specific CBVw fMRI responses to LOT stimulation that we previously observed (Poplawsky et al., 2019a, 2015).

## Acknowledgments

We thank Ping Wang for his experimental support and Dr. Mike Modo for kindly allowing us to use his cryostat. This work was supported by the National Institutes of Health (R01-NS094404 to A.V., R01-NS116450 to B.L., and R01-EB003324 to M.F.); and the Institute for Basic Science (Korea) (IBS-R15-D1 to S.G.K.). Corresponding author: Mitsuhiro Fukuda, mif5@pitt.edu; 3025 E Carson St, rm 159, Pittsburgh, PA 15203

## References

- Akgören N, Mathiesen C, Rubin I, Lauritzen M, 1997 Laminar analysis of activity-dependent increases of CBF in rat cerebellar cortex: dependence on synaptic strength. *Am. J. Physiol. Cell Physiol* 273 (3 Pt 2), H1166–H1176.
- Aksenov DP, Li L, Miller MJ, Wyrwicz AM, 2019 Role of the inhibitory system in shaping the BOLD fMRI response. *Neuroimage* 201, 116034 In press 10.1016/j.neuroimage.2019.116034. [PubMed: 31326573]
- Anenberg E, Chan AW, Xie Y, LeDue JM, Murphy TH, 2015 Optogenetic stimulation of GABA neurons can decrease local neuronal activity while increasing cortical blood flow. *J. Cereb. Blood Flow Metab* 35 (10), 1579–1586. [PubMed: 26082013]
- Aoki C, Rhee J, Lubin M, Dawson TM, 1997 NMDA-R1 subunit of the cerebral cortex co-localizes with neuronal nitric oxide synthase at pre- and postsynaptic sites and in spines. *Brain Res.* 750 (1), 25–40. [PubMed: 9098526]
- Aroniadou-Anderjaska V, Ennis M, Shipley MT, 1999 Dendrodendritic recurrent excitation in mitral cells of the rat olfactory bulb. *J. Neurophysiol* 82 (1), 489–494. [PubMed: 10400976]
- Aydin A–K, Haselden WD, Goulam Houssen Y, Pouzat C, Rungta RL, Demené C, Tanter M, Drew PJ, Charpak S, Boido D, 2020 Transfer functions linking neural calcium to single voxel functional ultrasound signal. *Nat. Commun* 11 (1), 2954. [PubMed: 32528069]
- Bardoni R, Magherini PC, Belluzzi O, 1996 Excitatory synapses in the glomerular triad of frog olfactory bulb in vitro. *Neuroreport* 7 (11), 1851–1855. [PubMed: 8905679]
- Bartel DL, Relá L, Hsieh L, Greer CA, 2015 Dendrodendritic synapses in the mouse olfactory bulb external plexiform layer. *J. Comp. Neurol* 523 (8), 1145–1161. [PubMed: 25420934]
- Blinder P, Tsai PS, Kaufhold JP, Knutsen PM, Suhl H, Kleinfeld D, 2013 The cortical angiome: an interconnected vascular network with noncolumnar patterns of blood flow. *Nat. Neurosci* 16 (7), 889–897. [PubMed: 23749145]
- Boorman L, Kennerley AJ, Johnston D, Jones M, Zheng Y, Redgrave P, Berwick J, 2010 Negative blood oxygen level dependence in the rat: a model for investigating the role of suppression in neurovascular coupling. *J. Neurosci* 30 (12), 4285–4294. [PubMed: 20335464]
- Borowsky IW, Collins RC, 1989 Metabolic anatomy of brain: a comparison of regional capillary density, glucose metabolism, and enzyme activities. *J. Comp. Neurol* 288 (3), 401–413. [PubMed: 2551935]
- Cauli B, Tong XK, Rancillac A, Serluca N, Lambolez B, Rossier J, Hamel E, 2004 Cortical GABA interneurons in neurovascular coupling: relays for subcortical vasoactive pathways. *J. Neurosci* 24 (41), 8940–8949. [PubMed: 15483113]
- Chaigneau E, Tiret P, Lecoq J, Ducros M, Knopfel T, Charpak S, 2007 The relationship between blood flow and neuronal activity in the rodent olfactory bulb. *J. Neurosci* 27 (24), 6452–6460. [PubMed: 17567806]
- Chen BR, Kozberg MG, Bouchard MB, Shaik MA, Hillman EM, 2014 A critical role for the vascular endothelium in functional neurovascular coupling in the brain. *J. Am. Heart Assoc* 3 (3), e000787. [PubMed: 24926076]
- Chen WR, Xiong W, Shepherd GM, 2000 Analysis of relations between NMDA receptors and GABA release at olfactory bulb reciprocal synapses. *Neuron* 25 (3), 625–633. [PubMed: 10774730]
- Dahlqvist MK, Thomsen KJ, Postnov DD, Lauritzen MJ, 2020 Modification of oxygen consumption and blood flow in mouse somatosensory cortex by cell-type-specific neuronal activity. *J. Cereb. Blood Flow Metab* 40 (10), 2010–2025. [PubMed: 31645177]
- De Saint Jan D, Westbrook GL, 2005 Detecting activity in olfactory bulb glomeruli with astrocyte recording. *J. Neurosci* 25 (11), 2917–2924. [PubMed: 15772351]
- Devor A, Hillman EM, Tian P, Waeber C, Teng IC, Ruvinskaya L, Shalinsky MH, Zhu H, Haslinger RH, Narayanan SN, Ulbert I, Dunn AK, Lo EH, Rosen BR, Dale AM, Kleinfeld D, Boas DA, 2008 Stimulus-induced changes in blood flow and 2-deoxyglucose uptake dissociate in ipsilateral somatosensory cortex. *J. Neurosci* 28 (53), 14347–14357. [PubMed: 19118167]

- Doengi M, Hirnet D, Coulon P, Pape HC, Deitmer JW, Lohr C, 2009 GABA uptake-dependent Ca(2+) signaling in developing olfactory bulb astrocytes. *Proc. Natl. Acad. Sci. U. S. A* 106 (41), 17570–17575. [PubMed: 19805126]
- Dragunow M, Faull R, 1989 The use of c-fos as a metabolic marker in neuronal pathway tracing. *J. Neurosci. Methods* 29 (3), 261–265. [PubMed: 2507830]
- Echagarruga CT, Gheres KW, Norwood JN, Drew PJ, 2020 nNOS-expressing interneurons control basal and behaviorally evoked arterial dilation in somatosensory cortex of mice. *eLife* 9 (e60533), 1–39.
- Enager P, Piilgaard H, Offenhauser N, Kocharyan A, Fernandes P, Hamel E, Lauritzen M, 2009 Pathway-specific variations in neurovascular and neurometabolic coupling in rat primary somatosensory cortex. *J. Cereb. Blood Flow Metab* 29 (5), 976–986. [PubMed: 19337274]
- Erlander MG, Tillakaratne NJ, Feldblum S, Patel N, Tobin AJ, 1991 Two genes encode distinct glutamate decarboxylases. *Neuron* 7 (1), 91–100. [PubMed: 2069816]
- Esclapez M, Tillakaratne NJ, Kaufman DL, Tobin AJ, Houser CR, 1994 Comparative localization of two forms of glutamic acid decarboxylase and their mRNAs in rat brain supports the concept of functional differences between the forms. *J. Neurosci* 14 (3 Pt 2), 1834–1855. [PubMed: 8126575]
- Filosa JA, Bonev AD, Straub SV, Meredith AL, Wilkerson MK, Aldrich RW, Nelson MT, 2006 Local potassium signaling couples neuronal activity to vasodilation in the brain. *Nat. Neurosci* 9 (11), 1397–1403. [PubMed: 17013381]
- Fredriksson I, Larsson M, Stromberg T, 2009 Measurement depth and volume in laser Doppler flowmetry. *Microvasc. Res* 78 (1), 4–13. [PubMed: 19285089]
- Freeman WJ, 1974 Relation of glomerular neuronal activity to glomerular transmission attenuation. *Brain Res.* 65 (1), 91–107. [PubMed: 4359029]
- Gall C, Seroogy KB, Brecha N, 1986 Distribution of VIP- and NPY-like immunoreactivities in rat main olfactory bulb. *Brain Res.* 374 (2), 389–394. [PubMed: 2424562]
- Girouard H, Bonev AD, Hannah RM, Meredith A, Aldrich RW, Nelson MT, 2010 Astrocytic endfoot Ca<sub>2</sub><sup>+</sup> and BK channels determine both arteriolar dilation and constriction. *Proc. Natl. Acad. Sci. U. S. A* 107 (8), 3811–3816. [PubMed: 20133576]
- Gsell W, Burke M, Wiedermann D, Bonvento G, Silva AC, Dauphin F, Buhle C, Hoehn M, Schwindt W, 2006 Differential effects of NMDA and AMPA glutamate receptors on functional magnetic resonance imaging signals and evoked neuronal activity during forepaw stimulation of the rat. *J. Neurosci* 26 (33), 8409–8416. [PubMed: 16914666]
- Gurden H, Uchida N, Mainen ZF, 2006 Sensory-evoked intrinsic optical signals in the olfactory bulb are coupled to glutamate release and uptake. *Neuron* 52 (2), 335–345. [PubMed: 17046695]
- Halabisky B, Friedman D, Radojicic M, Strowbridge BW, 2000 Calcium influx through NMDA receptors directly evokes GABA release in olfactory bulb granule cells. *J. Neurosci* 20 (13), 5124–5134. [PubMed: 10864969]
- Hamel E, 2006 Perivascular nerves and the regulation of cerebrovascular tone. *J. Appl. Physiol* 100 (3), 1059–1064. [PubMed: 16467392]
- Hardingham N, Dachtler J, Fox K, 2013 The role of nitric oxide in pre-synaptic plasticity and homeostasis. *Front. Cell Neurosci* 7 (190), 1–19. [PubMed: 23355802]
- Hogan-Cann AD, Lu P, Anderson CM, 2019 Endothelial NMDA receptors mediate activity-dependent brain hemodynamic responses in mice. *Proc. Natl. Acad. Sci. U. S. A* 116 (21), 10229–10231. [PubMed: 31061120]
- Hosford PS, Gourine AV, 2019 What is the key mediator of the neurovascular coupling response? *Neurosci. Biobehav. Rev* 96, 174–181. [PubMed: 30481531]
- Huber L, Handwerker DA, Jangraw DC, Chen G, Hall A, Stüber C, Gonzalez-Castillo J, Ivanov D, Marrett S, Guidi M, Goense J, Poser BA, Bandettini PA, 2017 High-resolution CBV-fMRI allows mapping of laminar activity and connectivity of cortical input and output in human M1. *Neuron* 96 (6), 1253–1263.e1257. [PubMed: 29224727]
- Husi H, Ward MA, Choudhary JS, Blackstock WP, Grant SGN, 2000 Proteomic analysis of NMDA receptor–adhesion protein signaling complexes. *Nat. Neurosci* 3 (7), 661–669. [PubMed: 10862698]

- Iadecola C, Yang G, Ebner TJ, Chen G, 1997 Local and propagated vascular responses evoked by focal synaptic activity in cerebellar cortex. *J. Neurophysiol* 78 (2), 651–659. [PubMed: 9307102]
- Igarashi KM, Ieki N, An M, Yamaguchi Y, Nagayama S, Kobayakawa K, Kobayakawa R, Tanifuji M, Sakano H, Chen WR, Mori K, 2012 Parallel mitral and tufted cell pathways route distinct odor information to different targets in the olfactory cortex. *J. Neurosci* 32 (23), 7970–7985. [PubMed: 22674272]
- Jordanova B, Vazquez A, Kozai TD, Fukuda M, Kim SG, 2018 Optogenetic investigation of the variable neurovascular coupling along the interhemispheric circuits. *J. Cereb. Blood Flow Metab* 38 (4), 627–640. [PubMed: 29372655]
- Jordanova B, Vazquez AL, Poplawsky AJ, Fukuda M, Kim SG, 2015 Neural and hemodynamic responses to optogenetic and sensory stimulation in the rat somatosensory cortex. *J. Cereb. Blood Flow Metab* 35 (6), 922–932. [PubMed: 25669905]
- Isaacson JS, Strowbridge BW, 1998 Olfactory reciprocal synapses: dendritic signaling in the CNS. *Neuron* 20 (4), 749–761. [PubMed: 9581766]
- Isaacson JS, Vitten H, 2003 GABA(B) receptors inhibit dendrodendritic transmission in the rat olfactory bulb. *J. Neurosci* 23 (6), 2032–2039. [PubMed: 12657661]
- Jahr CE, Nicoll RA, 1980 Dendrodendritic inhibition: demonstration with intracellular recording. *Science* 207 (4438), 1473–1475. [PubMed: 7361098]
- Jin T, Kim S–G, 2008 Cortical layer-dependent dynamic blood oxygenation, cerebral blood flow and cerebral blood volume responses during visual stimulation. *Neuroimage* 43 (1), 1–9. [PubMed: 18655837]
- Jukovskaya N, Tiret P, Lecoq J, Charpak S, 2011 What does local functional hyperemia tell about local neuronal activation? *J. Neurosci* 31 (5), 1579–1582. [PubMed: 21289165]
- Kennan RP, Scanley BE, Innis RB, Gore JC, 1998 Physiological basis for BOLD MR signal changes due to neuronal stimulation: separation of blood volume and magnetic susceptibility effects. *Magn. Reson. Med* 40 (6), 840–846. [PubMed: 9840828]
- Kishimoto J, Keverne EB, Hardwick J, Emson PC, 1993 Localization of nitric oxide synthase in the mouse olfactory and vomeronasal system: a histochemical, immuno-logical and in situ hybridization study. *Eur. J. Neurosci* 5 (12), 1684–1694. [PubMed: 7510206]
- Kocharyan A, Fernandes P, Tong XK, Vaucher E, Hamel E, 2008 Specific subtypes of cortical GABA interneurons contribute to the neurovascular coupling response to basal forebrain stimulation. *J. Cereb. Blood Flow Metab* 28 (2), 221–231. [PubMed: 17895909]
- Kosaka T, Kosaka K, 2007 Heterogeneity of nitric oxide synthase-containing neurons in the mouse main olfactory bulb. *Neurosci. Res* 57 (2), 165–178. [PubMed: 17134781]
- Kovacs KJ, 1998 c-Fos as a transcription factor: a stressful (re)view from a functional map. *Neurochem. Int* 33 (4), 287–297. [PubMed: 9840219]
- Krawchuk MB, Ruff CF, Yang X, Ross SE, Vazquez AL, 2020 Optogenetic assessment of VIP, PV, SOM and NOS inhibitory neuron activity and cerebral blood flow regulation in mouse somatosensory cortex. *J. Cereb. Blood Flow Metab* 40 (7), 1427–1440. [PubMed: 31418628]
- Laaris N, Puche A, Ennis M, 2007 Complementary postsynaptic activity patterns elicited in olfactory bulb by stimulation of mitral/tufted and centrifugal fiber inputs to granule cells. *J. Neurophysiol* 97 (1), 296–306. [PubMed: 17035366]
- Lalo U, Pankratov Y, Kirchhoff F, North RA, Verkhratsky A, 2006 NMDA receptors mediate neuron-to-glia signaling in mouse cortical astrocytes. *J. Neurosci* 26 (10), 2673–2683. [PubMed: 16525046]
- Lauritzen M, 2005 Reading vascular changes in brain imaging: is dendritic calcium the key? *Nat. Rev. Neurosci* 6 (1), 77–85. [PubMed: 15611729]
- Lecoq J, Tiret P, Najac M, Shepherd GM, Greer CA, Charpak S, 2009 Odor-evoked oxygen consumption by action potential and synaptic transmission in the olfactory bulb. *J. Neurosci* 29 (5), 1424–1433. [PubMed: 19193889]
- Leclux C, Toussay X, Kocharyan A, Fernandes P, Neupane S, Levesque M, Plaisier F, Shmuel A, Cauli B, Hamel E, 2011 Pyramidal neurons are “neurogenic hubs” in the neurovascular coupling response to whisker stimulation. *J. Neurosci* 31 (27), 9836–9847. [PubMed: 21734275]

- Lee L, Boorman L, Glendenning E, Christmas C, Sharp P, Redgrave P, Shabir O, Bracci E, Berwick J, Howarth C, 2020b Key Aspects of Neurovascular Control Mediated by Specific Populations of Inhibitory Cortical Interneurons. *Cereb. Cortex* 30 (4), 2452–2464. [PubMed: 31746324]
- Lee JH, Durand R, Gradinaru V, Zhang F, Goshen I, Kim DS, Fenno LE, Ramakrishnan C, Deisseroth K, 2010 Global and local fMRI signals driven by neurons defined optogenetically by type and wiring. *Nature* 465 (7299), 788–792. [PubMed: 20473285]
- Lee J, Stile CL, Bice AR, Rosenthal ZP, Yan P, Snyder AZ, Lee J–M, Bauer AQ, 2020a Opposed hemodynamic responses following increased excitation and parvalbumin-based inhibition. *J. Cereb. Blood Flow Metab* In press 10.1177/0271678X20930831.
- Li B, Gong L, Wu R, Li A, Xu F, 2014 Complex relationship between BOLD-fMRI and electrophysiological signals in different olfactory bulb layers. *Neuroimage* 95, 29–38. [PubMed: 24675646]
- Lledo P–M, Merkle FT, Alvarez-Buylla A, 2008 Origin and function of olfactory bulb interneuron diversity. *Trends Neurosci.* 31 (8), 392–400. [PubMed: 18603310]
- Logothetis NK, 2008 What we can do and what we cannot do with fMRI. *Nature* 453 (7197), 869–878. [PubMed: 18548064]
- Logothetis NK, Pauls J, Augath M, Trinath T, Oeltermann A, 2001 Neurophysiological investigation of the basis of the fMRI signal. *Nature* 412 (6843), 150–157. [PubMed: 11449264]
- Longden TA, Dabertrand F, Koide M, Gonzales AL, Tykocki NR, Brayden JE, Hill-Eubanks D, Nelson MT, 2017 Capillary K(+)-sensing initiates retrograde hyperpolarization to increase local cerebral blood flow. *Nat. Neurosci* 20 (5), 717–726. [PubMed: 28319610]
- Lu H, Golay X, Pekar JJ, Van Zijl PC, 2003 Functional magnetic resonance imaging based on changes in vascular space occupancy. *Magn. Reson. Med* 50 (2), 263–274. [PubMed: 12876702]
- Lu L, Hogan-Cann AD, Globa AK, Lu P, Nagy JI, Bamji SX, Anderson CM, 2019 Astrocytes drive cortical vasodilatory signaling by activating endothelial NMDA receptors. *J. Cereb. Blood Flow Metab* 39 (3), 481–496. [PubMed: 29072857]
- Luo M, Katz LC, 2001 Response correlation maps of neurons in the mammalian olfactory bulb. *Neuron* 32 (6), 1165–1179. [PubMed: 11754845]
- Lyons DG, Parpaleix A, Roche M, Charpak S, 2016 Mapping oxygen concentration in the awake mouse brain. *Elife* 5 (e12024), 1–16.
- Mahn M, Prigge M, Ron S, Levy R, Yizhar O, 2016 Biophysical constraints of optogenetic inhibition at presynaptic terminals. *Nat. Neurosci* 19 (4), 554–556. [PubMed: 26950004]
- Mandeville JB, Marota JJ, Kosofsky BE, Keltner JR, Weissleder R, Rosen BR, Weisskoff RM, 1998 Dynamic functional imaging of relative cerebral blood volume during rat forepaw stimulation. *Magn. Reson. Med* 39 (4), 615–624. [PubMed: 9543424]
- Masamoto K, Kim T, Fukuda M, Wang P, Kim SG, 2007 Relationship between neural, vascular, and BOLD signals in isoflurane-anesthetized rat somatosensory cortex. *Cereb. Cortex* 17 (4), 942–950. [PubMed: 16731882]
- Mathiesen C, Caesar K, Akgoren N, Lauritzen M, 1998 Modification of activity-dependent increases of cerebral blood flow by excitatory synaptic activity and spikes in rat cerebellar cortex. *J. Physiol* 512 (2), 555–566. [PubMed: 9763643]
- Mayer B, Schmid M, Klatt P, Schmidt K, 1993 Reversible inactivation of endothelial nitric oxide synthase by NG-nitro-L-arginine. *FEBS Lett.* 333 (1–2), 203–206. [PubMed: 7693510]
- McQuade LE, Ma J, Lowe G, Ghatpande A, Gelperin A, Lippard SJ, 2010 Visualization of nitric oxide production in the mouse main olfactory bulb by a cell-trappable copper(II) fluorescent probe. *Proc. Natl. Acad. Sci. U. S. A* 107 (19), 8525. [PubMed: 20413724]
- Miller JE, Granados-Fuentes D, Wang T, Marpegan L, Holy TE, Herzog ED, 2014 Vasoactive intestinal polypeptide mediates circadian rhythms in mammalian olfactory bulb and olfaction. *J. Neurosci* 34 (17), 6040–6046. [PubMed: 24760863]
- Mishra A, Reynolds JP, Chen Y, Gourine AV, Rusakov DA, Attwell D, 2016 Astrocytes mediate neurovascular signaling to capillary pericytes but not to arterioles. *Nat. Neurosci* 19 (12), 1619–1627. [PubMed: 27775719]
- Mori K, Takagi SF, 1978 An intracellular study of dendrodendritic inhibitory synapses on mitral cells in the rabbit olfactory bulb. *J. Physiol* 279, 569–588. [PubMed: 671363]

- Nagayama S, Homma R, Imamura F, 2014 Neuronal organization of olfactory bulb circuits. *Front. Neural Circuits* 8, 98. [PubMed: 25232305]
- Nagel G, Szellas T, Huhn W, Kateriya S, Adeishvili N, Berthold P, Ollig D, Hegemann P, Bamberg E, 2003 Channelrhodopsin-2, a directly light-gated cation-selective membrane channel. *Proc. Natl. Acad. Sci. U. S. A* 100 (24), 13940–13945. [PubMed: 14615590]
- Nakashima M, Mori K, Takagi SF, 1978 Centrifugal influence on olfactory bulb activity in the rabbit. *Brain Res.* 154 (2), 301–306. [PubMed: 687996]
- Nicoll RA, 1969 Inhibitory mechanisms in the rabbit olfactory bulb: dendrodendritic mechanisms. *Brain Res.* 14 (1), 157–172. [PubMed: 5783107]
- Nielsen AN, Lauritzen M, 2001 Coupling and uncoupling of activity-dependent increases of neuronal activity and blood flow in rat somatosensory cortex. *J. Physiol* 533 (Pt 3), 773–785. [PubMed: 11410634]
- Octeau JC, Gangwani MR, Allam SL, Tran D, Huang S, Hoang-Trong TM, Golshani P, Rumbell TH, Kozloski JR, Khakh BS, 2019 Transient, consequential increases in extracellular potassium ions accompany channelrhodopsin2 excitation. *Cell Rep.* 27 (8), 2249–2261. [PubMed: 31116972]
- Otsu Y, Couchman K, Lyons DG, Collot M, Agarwal A, Mallet JM, Pfrieger FW, Bergles DE, Charpak S, 2015 Calcium dynamics in astrocyte processes during neurovascular coupling. *Nat. Neurosci* 18 (2), 210–218. [PubMed: 25531572]
- Owen SF, Liu MH, Kreitzer AC, 2019 Thermal constraints on in vivo optogenetic manipulations. *Nat. Neurosci* 22 (7), 1061–1065. [PubMed: 31209378]
- Petzold GC, Albeanu DF, Sato TF, Murthy VN, 2008 Coupling of neural activity to blood flow in olfactory glomeruli is mediated by astrocytic pathways. *Neuron* 58 (6), 897–910. [PubMed: 18579080]
- Poplawsky AJ, Fukuda M, Kang BM, Kim JH, Suh M, Kim SG, 2019a Dominance of layer-specific microvessel dilation in contrast-enhanced high-resolution fMRI: comparison between hemodynamic spread and vascular architecture with CLARITY. *Neuroimage* 197, 657–667. [PubMed: 28822749]
- Poplawsky AJ, Fukuda M, Kim SG, 2019b Foundations of layer-specific fMRI and investigations of neurophysiological activity in the laminarized neocortex and olfactory bulb of animal models. *Neuroimage* 199, 718–729. [PubMed: 28502845]
- Poplawsky AJ, Fukuda M, Murphy M, Kim SG, 2015 Layer-specific fMRI responses to excitatory and inhibitory neuronal activities in the olfactory bulb. *J. Neurosci* 35 (46), 15263–15275. [PubMed: 26586815]
- Poplawsky AJ, Kim SG, 2014 Layer-dependent BOLD and CBV-weighted fMRI responses in the rat olfactory bulb. *Neuroimage* 91, 237–251. [PubMed: 24418506]
- Price JL, Powell TP, 1970 The synaptology of the granule cells of the olfactory bulb. *J. Cell Sci* 7 (1), 125–155. [PubMed: 5476853]
- Raimondo JV, Kay L, Ellender TJ, Akerman CJ, 2012 Optogenetic silencing strategies differ in their effects on inhibitory synaptic transmission. *Nat. Neurosci* 15 (8), 1102–1104. [PubMed: 22729174]
- Rall W, Shepherd GM, 1968 Theoretical reconstruction of field potentials and dendrodendritic synaptic interactions in olfactory bulb. *J. Neurophysiol* 31 (6), 884–915. [PubMed: 5710539]
- Rall W, Shepherd GM, Reese TS, Brightman MW, 1966 Dendrodendritic synaptic pathway for inhibition in the olfactory bulb. *Exp. Neurol* 14 (1), 44–56. [PubMed: 5900523]
- Rancillac A, Rossier J, Guille M, Tong XK, Geoffroy H, Amatore C, Arbault S, Hamel E, Cauli B, 2006 Glutamatergic control of microvascular tone by distinct GABA neurons in the cerebellum. *J. Neurosci* 26 (26), 6997–7006. [PubMed: 16807329]
- Rungta RL, Chaigneau E, Osmanski BF, Charpak S, 2018 Vascular compartmentalization of functional hyperemia from the synapse to the pia. *Neuron* 99 (2), 362–375. [PubMed: 29937277]
- Rungta RL, Osmanski BF, Boido D, Tanter M, Charpak S, 2017 Light controls cerebral blood flow in naive animals. *Nat. Commun* 8, 14191. [PubMed: 28139643]
- Sassoe-Pognetto M, Ottersen OP, 2000 Organization of ionotropic glutamate receptors at dendrodendritic synapses in the rat olfactory bulb. *J. Neurosci* 20 (6), 2192–2201. [PubMed: 10704494]

- Schoppa NE, Kinzie JM, Sahara Y, Segerson TP, Westbrook GL, 1998 Dendrodendritic inhibition in the olfactory bulb is driven by NMDA receptors. *J. Neurosci* 18 (17), 6790–6802. [PubMed: 9712650]
- Schulz K, Sydekum E, Krueppel R, Engelbrecht CJ, Schlegel F, Schröter A, Rudin M, Helmchen F, 2012 Simultaneous BOLD fMRI and fiber-optic calcium recording in rat neocortex. *Nat. Methods* 9 (6), 597–602. [PubMed: 22561989]
- Spessert R, Wohlgemuth C, Reuss S, Layes E, 1994 NADPH-diaphorase activity of nitric oxide synthase in the olfactory bulb: co-factor specificity and characterization regarding the interrelation to NO formation. *J. Histochem. Cytochem* 42 (5), 569–575. [PubMed: 7512584]
- Stefanovic B, Schwindt W, Hoehn M, Silva AC, 2007 Functional uncoupling of hemodynamic from neuronal response by inhibition of neuronal nitric oxide synthase. *J. Cereb. Blood Flow Metab* 27 (4), 741–754. [PubMed: 16883353]
- Sun W, McConnell E, Pare JF, Xu Q, Chen M, Peng W, Lovatt D, Han X, Smith Y, Nedergaard M, 2013 Glutamate-dependent neuroglial calcium signaling differs between young and adult brain. *Science* 339 (6116), 197–200. [PubMed: 23307741]
- Taniguchi H, 2014 Genetic dissection of GABAergic neural circuits in mouse neocortex. *Front. Cell Neurosci* 8, 8. [PubMed: 24478631]
- Tian P, Teng IC, May LD, Kurz R, Lu K, Scadeng M, Hillman EM, De Crespigny AJ, D'Arceuil HE, Mandeville JB, Marota JJ, Rosen BR, Liu TT, Boas DA, Buxton RB, Dale AM, Devor A, 2010 Cortical depth-specific microvascular dilation underlies laminar differences in blood oxygenation level-dependent functional MRI signal. *Proc. Natl. Acad. Sci. U. S. A* 107 (34), 15246–15251. [PubMed: 20696904]
- Uhlirova H, et al., 2016 Cell type specificity of neurovascular coupling in cerebral cortex. *Elife* 5.
- Urban A, Rancillac A, Martinez L, Rossier J, 2012 Deciphering the neuronal circuitry controlling local blood flow in the cerebral cortex with optogenetics in PV::CRE transgenic mice. *Front. Pharmacol* 3, 105. [PubMed: 22715327]
- Utsumi M, Ohno K, Onchi H, Sato K, Tohyama M, 2001 Differential expression patterns of three glutamate transporters (GLAST, GLT1 and EAAC1) in the rat main olfactory bulb. *Mol. Brain Res* 92 (1–2), 1–11. [PubMed: 11483236]
- Uva L, Strowbridge BW, de Curtis M, 2006 Olfactory bulb networks revealed by lateral olfactory tract stimulation in the in vitro isolated guinea-pig brain. *Neuroscience* 142 (2), 567–577. [PubMed: 16887275]
- van Bruggen N, Busch E, Palmer JT, Williams SP, de Crespigny AJ, 1998 High-resolution functional magnetic resonance imaging of the rat brain: mapping changes in cerebral blood volume using iron oxide contrast media. *J. Cereb. Blood Flow Metab* 18 (11), 1178–1183. [PubMed: 9809506]
- Vaucher E, Tong XK, Cholet N, Lantin S, Hamel E, 2000 GABA neurons provide a rich input to microvessels but not nitric oxide neurons in the rat cerebral cortex: a means for direct regulation of local cerebral blood flow. *J. Comp. Neurol* 421 (2), 161–171. [PubMed: 10813779]
- Vazquez AL, Fukuda M, Crowley JC, Kim SG, 2014 Neural and hemodynamic responses elicited by forelimb- and photo-stimulation in channelrhodopsin-2 mice: insights into the hemodynamic point spread function. *Cereb. Cortex* 24 (11), 2908–2919. [PubMed: 23761666]
- Vazquez AL, Fukuda M, Kim SG, 2018 Inhibitory neuron activity contributions to hemodynamic responses and metabolic load examined using an inhibitory optogenetic mouse model. *Cereb. Cortex* 28 (11), 4105–4119. [PubMed: 30215693]
- Vincis R, Lagier S, Van De Ville D, Rodriguez I, Carleton A, 2015 Sensory-evoked intrinsic imaging signals in the olfactory bulb are independent of neurovascular coupling. *Cell Rep.* 12 (2), 313–325. [PubMed: 26146075]
- Viswanathan A, Freeman RD, 2007 Neurometabolic coupling in cerebral cortex reflects synaptic more than spiking activity. *Nat. Neurosci* 10 (10), 1308–1312. [PubMed: 17828254]
- Weber B, Keller AL, Reichold J, Logothetis NK, 2008 The microvascular system of the striate and extrastriate visual cortex of the macaque. *Cereb. Cortex* 18 (10), 2318–2330. [PubMed: 18222935]
- Wellis DP, Scott JW, 1990 Intracellular responses of identified rat olfactory bulb interneurons to electrical and odor stimulation. *J. Neurophysiol* 64 (3), 932–947. [PubMed: 2230935]

- Wells JA, Christie IN, Hosford PS, Huckstepp RT, Angelova PR, Vihko P, Cork SC, Abramov AY, Teschemacher AG, Kasparov S, Lythgoe MF, Gourine AV, 2015 A critical role for purinergic signalling in the mechanisms underlying generation of BOLD fMRI responses. *J. Neurosci* 35 (13), 5284–5292. [PubMed: 25834053]
- Weruaga E, Briñón JG, Porteros A, Arévalo R, Aijón J, Alonso JR, 2000 Expression of neuronal nitric oxide synthase/NADPH-diaphorase during olfactory deaf-ferentation and regeneration. *Eur. J. Neurosci* 12 (4), 1177–1193. [PubMed: 10762349]
- Wilson DA, Sullivan RM, Gall CM, Guthrie KM, 1996 NMDA-receptor modulation of lateral inhibition and c-fos expression in olfactory bulb. *Brain Res.* 719 (1–2), 62–71. [PubMed: 8782864]
- Witthoft A, Filosa JA, Karniadakis GE, 2013 Potassium buffering in the neurovascular unit: models and sensitivity analysis. *Biophys. J* 105 (9), 2046–2054. [PubMed: 24209849]
- Xiong W, Chen WR, 2002 Dynamic gating of spike propagation in the mitral cell lateral dendrites. *Neuron* 34 (1), 115–126. [PubMed: 11931746]
- Yokoi M, Mori K, Nakanishi S, 1995 Refinement of odor molecule tuning by dendrodendritic synaptic inhibition in the olfactory bulb. *Proc. Natl. Acad. Sci. U. S. A* 92 (8), 3371–3375. [PubMed: 7724568]
- Zhao F, Wang X, Zariwala HA, Uslaner JM, Houghton AK, Evelhoch JL, Hostetler E, Winkelmann CT, Hines CDG, 2017 fMRI study of the role of glutamate NMDA receptor in the olfactory adaptation in rats: insights into cellular and molecular mechanisms of olfactory adaptation. *Neuroimage* 149, 348–360. [PubMed: 28163142]
- Zhao S, Ting JT, Atallah HE, Qiu L, Tan J, Gloss B, Augustine GJ, Deisseroth K, Luo M, Graybiel AM, Feng G, 2011 Cell type-specific channelrhodopsin-2 transgenic mice for optogenetic dissection of neural circuitry function. *Nat. Methods* 8 (9), 745–752. [PubMed: 21985008]
- Zong X, Lee J, John Poplawsky A, Kim SG, Ye JC, 2014 Compressed sensing fMRI using gradient-recalled echo and EPI sequences. *Neuroimage* 92, 312–321. [PubMed: 24495813]

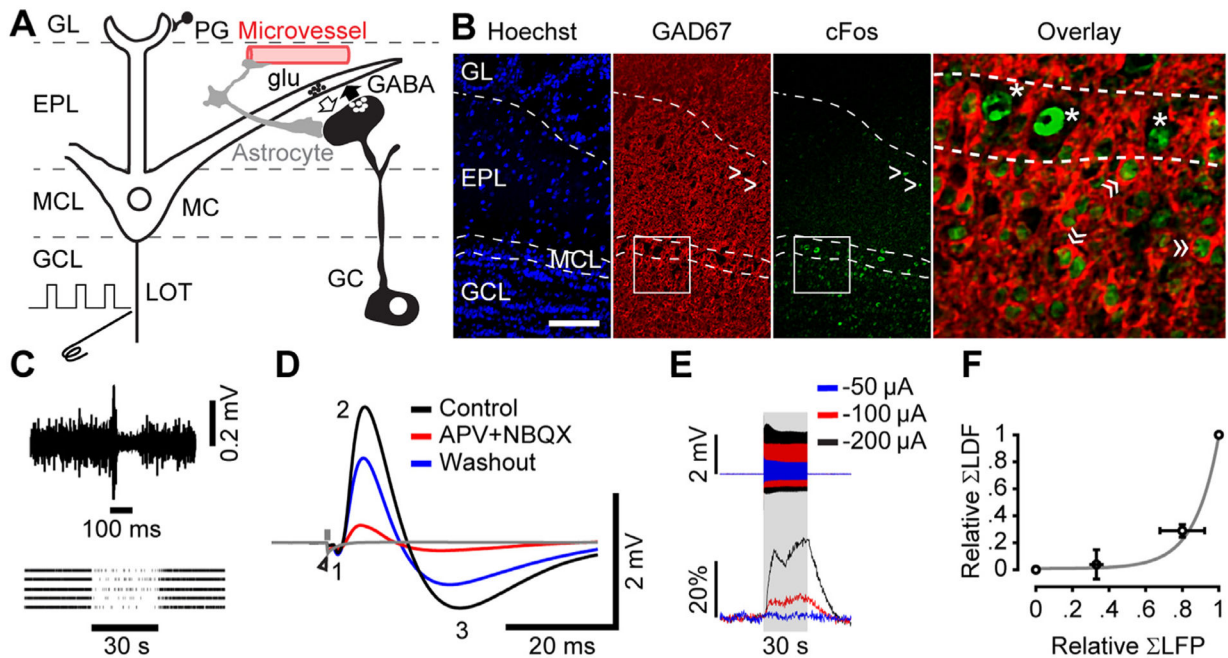


**Fig. 1. LOT stimulation targets inhibitory granule cell activation.**

(A) Schematic of the stimulation paradigm. Axons of excitatory mitral cells (MC) in MCL form the white matter tract, LOT. Electrical stimulation of LOT produces antidromic action potentials that return to the mitral cell bodies and excite inhibitory granule cells (GC, bodies in GCL) via reciprocal dendrodendritic synapses in EPL, where glutamate and GABA release sites are closely apposed. At the reciprocal synapses, glutamate (glu, black circles) is released from the lateral dendrites of MCs onto the GC spines (white arrow) and GABA (white circles) is released from the same spine back onto the lateral dendrites (black arrow). An astrocyte hypothetically bridges the dendrodendritic synapse and microvessel. (B) Triple immunohistochemical histological staining (Hoescht for all cell nuclei, GAD<sub>67</sub> for inhibitory neurons, c-Fos for nuclei with increased metabolism, overlay: white square regions on GAD<sub>67</sub> and c-Fos images are overlaid and enlarged) verifies that LOT stimulation (10-s pulsed train of  $-150\ \mu\text{A}$ ,  $100\text{-}\mu\text{s}$  duration,  $40\text{-Hz}$  pulses;  $30\text{-s}$  interstimulus interval for  $90\text{ min}$ ) increased c-Fos activity in inhibitory GCs located in GCL ( $\llcorner$ , green c-Fos positive nuclei, red cytosolic GAD<sub>67</sub> positive). MCs in MCL ( $\ast$ , GAD<sub>67</sub> negative) also had increased c-Fos activity due to direct stimulation; similar to a few tufted cells in EPL ( $\triangleright$ , GAD<sub>67</sub> negative). Dendrodendritic synapses of periglomerular cells (PG) were not activated much by LOT stimulation.  $100\text{-}\mu\text{m}$  scale bar. (C) (Top) LOT stimulation (black horizontal bar) caused a prolonged ( $\sim 100\text{ ms}$ ) suppression of spontaneous MUAs in EPL/MCL (single sweep), indicating that inhibitory processes are preferentially evoked. (Bottom) Spike raster plots for 5 runs. Spontaneous spiking activity recorded from EPL is suppressed during a  $30\text{-s}$ ,  $40\text{-Hz}$  LOT stimulation. (D) Single-pulse stimulation of LOT (vertical gray line, a negative rectangular stimulus pulse with a  $200\text{-}\mu\text{A}$  amplitude,  $100\text{-}\mu\text{s}$  duration, and  $1\text{-Hz}$  frequency, average of 100 runs) evoked a signature triphasic LFP in GCL (black line). The amplitudes of the second and third phases decreased with dorsal application of ionotropic glutamate receptor antagonists (red line, a mixture of  $5\text{-mM}$  NBQX and  $25\text{-mM}$  APV for  $120\text{ min}$ ) that recovered with drug washout (blue line,  $120\text{ min}$ ), verifying that these LFP

phases originate from postsynaptic granule cell depolarization. The gray line shows the electrical stimulus artifact (arrowhead) caused by LOT stimulation after euthanasia. The gray vertical tick indicates stimulus onset. Traces are averages of 100 runs. (E) LOT was stimulated for 30 s at either  $-50$  (blue trace),  $-100$  (red), or  $-200$   $\mu\text{A}$  (black) in a pseudorandomized order (40 Hz, 100- $\mu\text{s}$  pulse width) every 120 s and repeated five times for each current. Time courses of LFP (top) and LDF responses (bottom) are averaged over 5 rats. (F) Relationship between the evoked LFP amplitude and LDF responses in E. Both LDF and LFP data obtained from individual currents were normalized by their values obtained at  $-200$   $\mu\text{A}$ . The sum of the area under the LDF responses has an exponential relationship with the sum of the area of LFP responses during LOT stimulation. Error bars, SE.

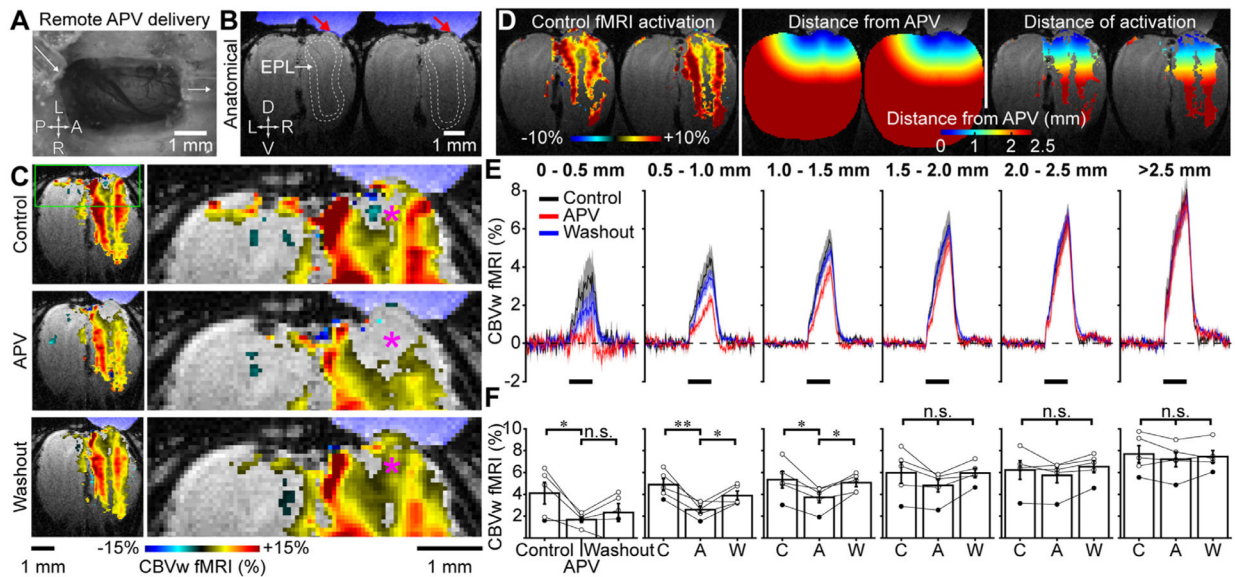


**Fig. 2. CBVw-fMRI responses to LOT stimulation decreased as a function of distance from the APV application site.**

The purpose of 25-mM APV application was to block NMDA receptors on inhibitory granule cells and decrease their postsynaptic activity ( $n = 5$  rats). (A) Remote application and washout of APV. Magnified image of the sealed chamber over the right olfactory bulb that contained the craniotomy with intact dura. Saline vehicle or APV was gravity fed through a 1.5 m inlet tube that flowed over the exposed bulb and exited through a second outlet tube in the direction of the white arrows. (B) Fast spin-echo anatomical image of the rat olfactory bulb showing the interface (red arrows) between the sealed chamber containing the saline or drug (blue) and the bulb. EPL anatomically forms a ring in coronal slices, which was approximately outlined by the dotted white lines using GL and MCL as guides since these layers appear hypointense in the T2-weighted images. Sensitivity decreases away from the 10-mm inner-diameter surface coil limit the accuracy of the EPL delineation in ventral bulb. (C, left column) CBVw-fMRI activation maps ( $p < 0.01$  voxel-wise and family-wise error corrected; 1 of 9 slices shown) to LOT stimulation during control (11 concatenated LOT-stimulation runs,  $df = 1663$ ; first row), 90-min APV application (17 runs,  $df = 2575$ ; second row), and 180-min washout periods (32 runs,  $df = 4855$ ; third row) from a representative rat (Rat 2). (C, right column) Expanded view of the dorsal surface of the bulb from the same position marked by the green rectangle in the control image. See the disappearance of dorsal fMRI activations nearest to the drug application site (blue) after APV application and its recovery following drug washout (marked by \*). Note, farther fMRI activations remained intact for these three conditions, confirming that topical drug application only had a local effect. (D) fMRI activation maps to LOT stimulation during the control period (left,  $p < 0.01$  voxel-wise and family-wise error correction, 2 of 9 slices shown, 10 concatenated runs,  $df = 1511$ , example data from Rat 4) were binned by the shortest Euclidean distance from the drug contact at the bulb surface (middle) to generate fMRI activation maps as a function of distance from the drug application site (right). (E) Mean time courses and (F) mean percent signal changes from all 9 slices for control (black traces), 25-mM APV (red), and washout (blue) periods at different binned locations (see

examples in D,  $n = 5$  rats). Linked circles in all bar graphs represent data from individual rats. NB: Rat 3 had the smallest responses evoked by LOT stimulation during the control period (filled circles in F; see also Fig. 3). \*  $p < 0.05$ , \*\*  $p < 0.01$ , n.s. not significant. L: left, R: right, A: anterior, P: posterior, D: dorsal, V: ventral.

Author Manuscript

Author Manuscript

Author Manuscript

Author Manuscript

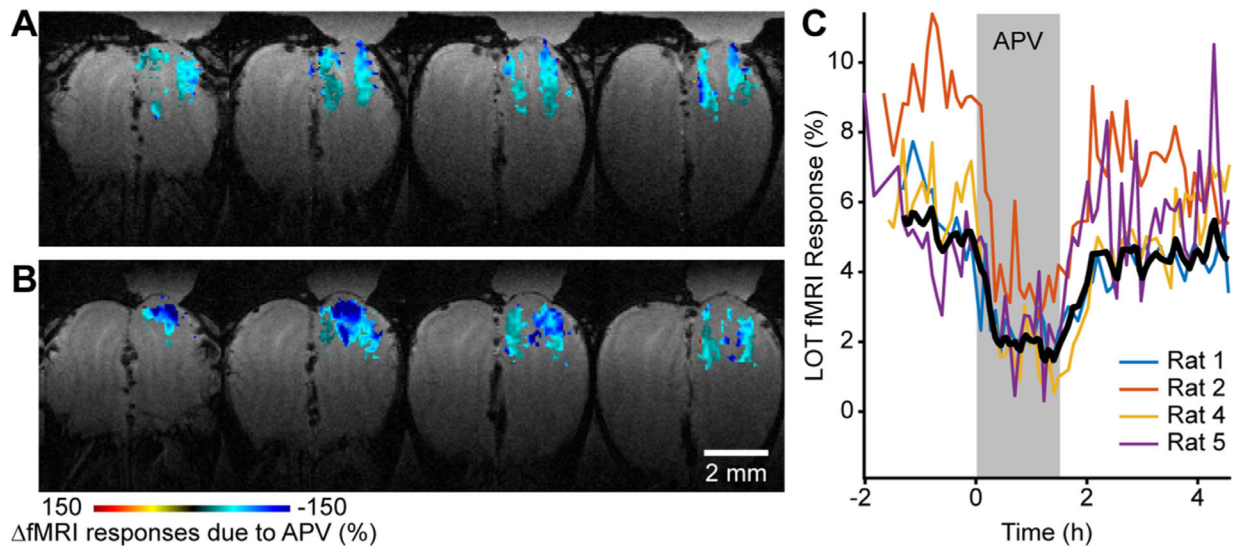


**Fig. 3. Voxel-wise and temporal effects of APV on evoked fMRI responses.**

Spatial mapping of APV effects using a linear regression analysis: Response variable, primary GLM fMRI percent change maps to individual LOT stimulations in time; predictor variable, simple block design whereby the pre-drug control and washout periods were “off” conditions and the 25-mM APV application period was “on”. Therefore, a condition of the analysis was that the responses following washout recovered to the same level as the pre-drug control. Only voxels that had significant responses evoked by LOT stimulation during the pre-drug control period ( $p < 0.01$  voxel- and family-wise error corrected) were included in this analysis and only voxels significantly affected by APV were shown (A – B) or analyzed further (C) ( $p < 0.05$  voxel- and family-wise error corrected). (A – B) Percent change maps due to APV calculated in Rats 2 (A,  $df = 62$ ) and 4 (B,  $df = 61$ ). These representative rats both showed deactivation due to APV confined to regions proximal to the drug application site, but with varying degrees of deactivation at the dorsal surface of the bulb, likely due to differences in the degree of recovery from APV. No significant voxels were observed in Rat 3 (see also Fig. 2F, filled circles), but subthreshold deactivation was noted. No deactivations were observed anywhere in the bulb beyond 2.5 mm from the drug application site or in noise regions outside of the bulb, which confirmed adequate control of type-1 error. (C) Average individual (colored lines) and group (black line,  $n = 4$  rats) time courses of the significant voxels from all 9 slices.

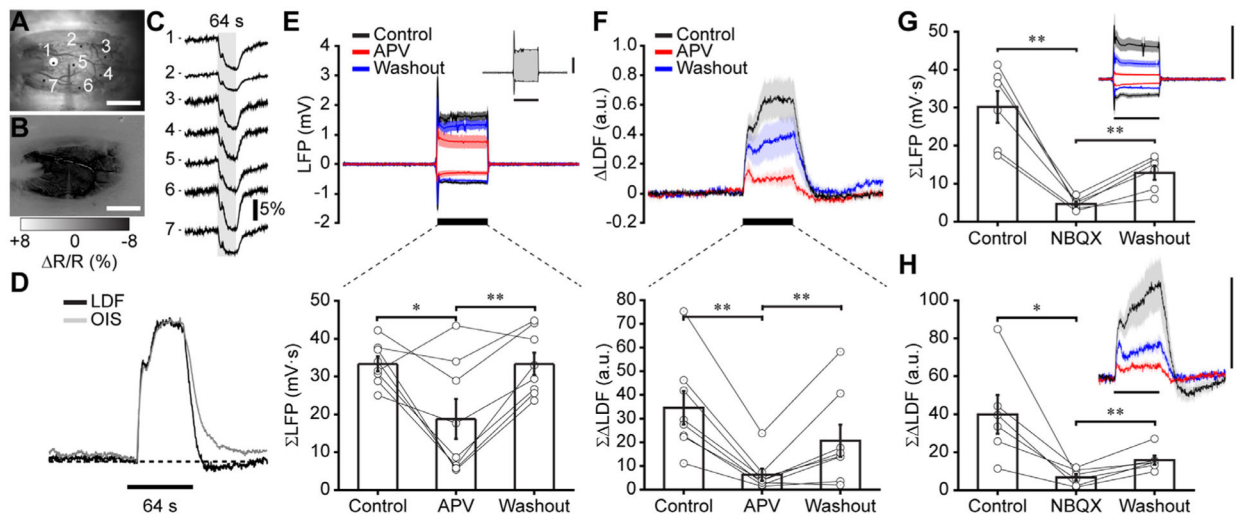


**Fig. 4. Blood flow responses evoked by inhibitory neurons decreased with glutamate receptor antagonists.**

The purposes of the separate application of 25-mM APV (E – F) or 5-mM NBQX (G – H) were to block NMDA or AMPA receptors on inhibitory granule cells, respectively, and decrease their postsynaptic activity ( $n = 8$  rats for APV,  $n = 6$  rats for NBQX). (A) Baseline optical intrinsic signal (OIS) image showing location of LDF probe tip near location “1” and an OIS region for comparison to LDF responses in D (white circle, radius = 10 pixels, ~125–160  $\mu\text{m}$  depending on magnification). A metal electrode for electrophysiological recordings appeared as a gray shadow with its tip near location “5”. Scale bars in A and B, 1 mm. (B) Average 572-nm OIS image during LOT stimulation (0–64 s after stimulus onset). (C) OIS time courses from seven locations across the bulb indicated in A. Decreased signal with stimulation indicates blood volume increases (vasodilation or increased total hemoglobin content). (D) Average of the concurrent OIS (gray) and LDF (black) measurements from 8 rats. To examine the dynamic properties of the CBF and CBV changes, their mean time courses were normalized by their peak intensities. Note that LDF data were down-sampled to a 2-Hz resolution in the same way as OIS. (E – F) Mean time-dependent LFP signals measured in GCL (E, top) or LDF relative changes ( $\Delta\text{LDF}$ ) measured on the bulb surface (F, top) to 64-s trains of LOT stimulation and the means of the sums of the area under the curves for LFP ( $\Sigma\text{LFP}$ ) (E, bottom) or  $\Delta\text{LDF}$  ( $\Sigma\Delta\text{LDF}$ ) (F, bottom) signals for the entire 64-s LOT stimulation during pre-drug control (black), APV-applied (red) and washout (blue) periods. Both LFP and LDF responses significantly decreased with APV application. (Inset in E) raw LFP signals (gray traces) and its envelope (black traces). Horizontal and vertical bars, 64 s and 1 mV, respectively. (G – H) Mean time-dependent LFP (G, inset) or  $\Delta\text{LDF}$  (H, inset) signals and mean evoked  $\Sigma\text{LFP}$  (G) or  $\Sigma\Delta\text{LDF}$  (H) signals during LOT stimulation for pre-drug control (black), NBQX-applied (red), and washout (blue) periods. Both LFP and LDF responses significantly decreased with NBQX. Horizontal and vertical bars in G inset, 64 s and 2 mV, respectively. Horizontal and vertical bars in H inset, 64 s and 0.8 (a.u.), respectively. \*  $p < 0.05$ , \*\*  $p < 0.01$ , a.u. arbitrary units.

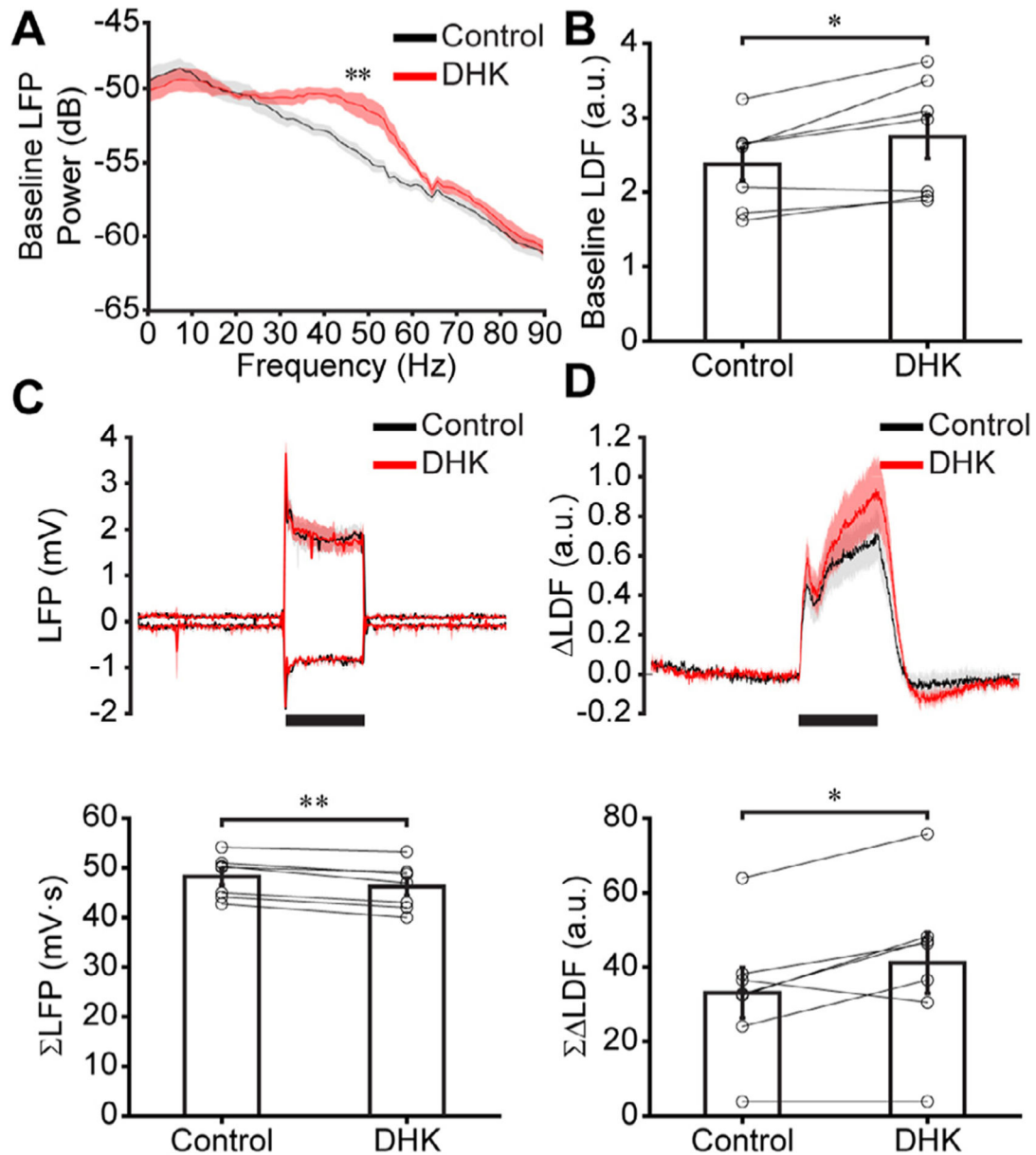


**Fig. 5. Glutamate reuptake by astrocytes contributed little to the evoked blood flow response.** The purpose of 1-mM DHK application was to block glutamate transporter-1 and inhibit glutamate reuptake by astrocytes ( $n = 7$  rats). (A) Mean power spectra of baseline LFPs during control (black) and application of DHK (red). Mostly low-gamma frequencies (30–50 Hz) significantly increased with DHK. (B) Baseline LDF signals significantly increased with DHK. (C – D) Mean time-dependent LFP (C, top) or LDF (D, top) signals and mean  $\Sigma$ LFP (C, bottom) and  $\Sigma$  LDF (D, bottom) responses to LOT stimulation for pre-drug control (black) and DHK application (red) periods. DHK slightly decreased the evoked LFP responses, but did not suppress the evoked LDF responses. \*  $p < 0.05$ , \*\*  $p < 0.01$ , a.u. arbitrary units.

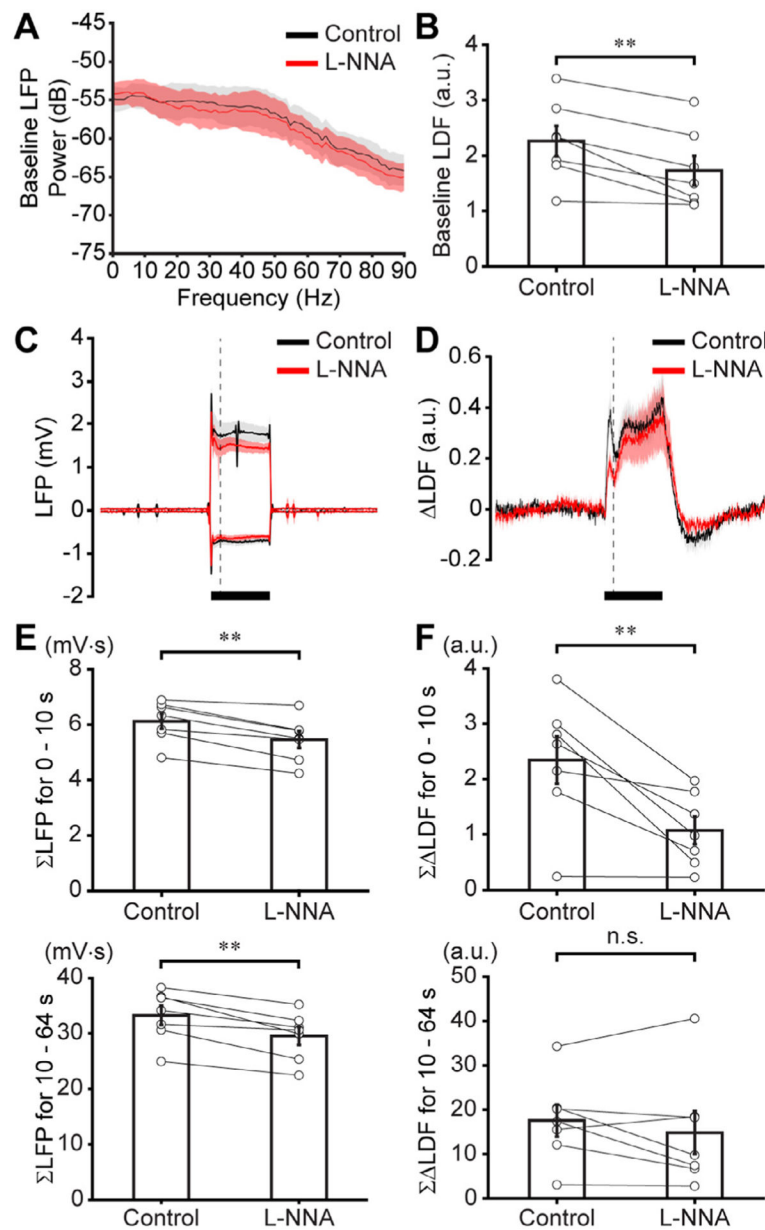


**Fig. 6. Nitric oxide contributed more to the initial, fast blood flow response.**

The purpose of 1-mM L-NNA application was to non-selectively and irreversibly inhibit nitric oxide synthase in neurons and vessels ( $n = 7$  rats). (A) Power spectra of baseline LFPs before (black) and after a 90-min application of L-NNA (red) were not significantly different; while (B) baseline LDF signals significantly decreased. Mean time-dependent (C) LFP and (D) LDF signals to LOT stimulation before (black) and after L-NNA application (red). Note, L-NNA appeared to preferentially decrease the initial, fast blood flow response. (E-F) Mean  $\Sigma$ LFP (E) or  $\Sigma$  LDF (F) responses for the initial 10-s (top) and following 54-s (bottom) bins during LOT stimulation for pre-drug control (black) and L-NNA-application (red) periods.  $\Sigma$ LFP significantly decreased with L-NNA during both time bins (top and

bottom), while  $\Sigma$  LDF significantly decreased only during the early 0–10-s (top) and not the later 10–64-s bin (bottom). \*\*  $p < 0.01$ , n.s. not significant, a.u. arbitrary units.

Author Manuscript

Author Manuscript

Author Manuscript

Author Manuscript

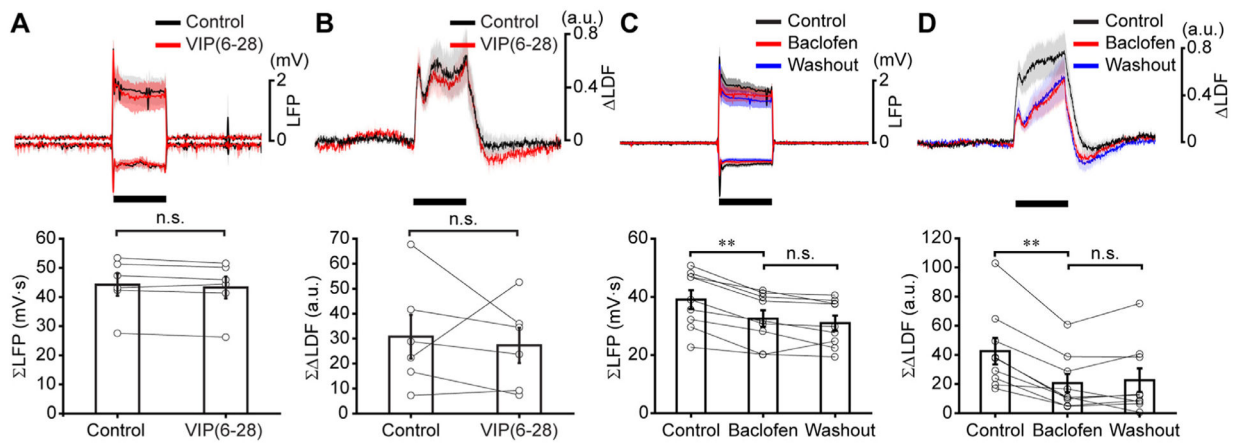


**Fig. 7. While vasoactive intestinal peptide did not mediate the blood flow responses to LOT stimulation, suppression of GABA release from inhibitory granule cells decreased the blood flow responses.**

The purpose of 0.1-mM VIP (6–28) application was to block VIP receptors on neurons and vessels and inhibit the associated vascular reactions ( $n = 6$  rats), while the purpose of 10-mM baclofen application was to activate GABA<sub>B</sub> autoreceptors on inhibitory granule cells and inhibit their presynaptic release of GABA ( $n = 9$  rats). (A–B) For VIP (6–28), mean time-dependent LFP (A, top) or LDF (B, top) signals and mean  $\Sigma$ LFP (A, bottom) or  $\Sigma$  LDF (B, bottom) responses evoked by LOT stimulation for pre-drug control (black) and VIP (6–28) application (red) periods. (C–D) For baclofen, mean time-dependent LFP (C, top) or LDF (D, top) signals and mean  $\Sigma$ LFP (C, bottom) or  $\Sigma$  LDF (D, bottom) responses evoked by LOT stimulation for pre-drug control (black), baclofen application (red), and washout (blue) periods. Both LFP and LDF responses significantly decreased with baclofen application, but did not significantly recover. \*\*  $p < 0.01$ , n.s. not significant.

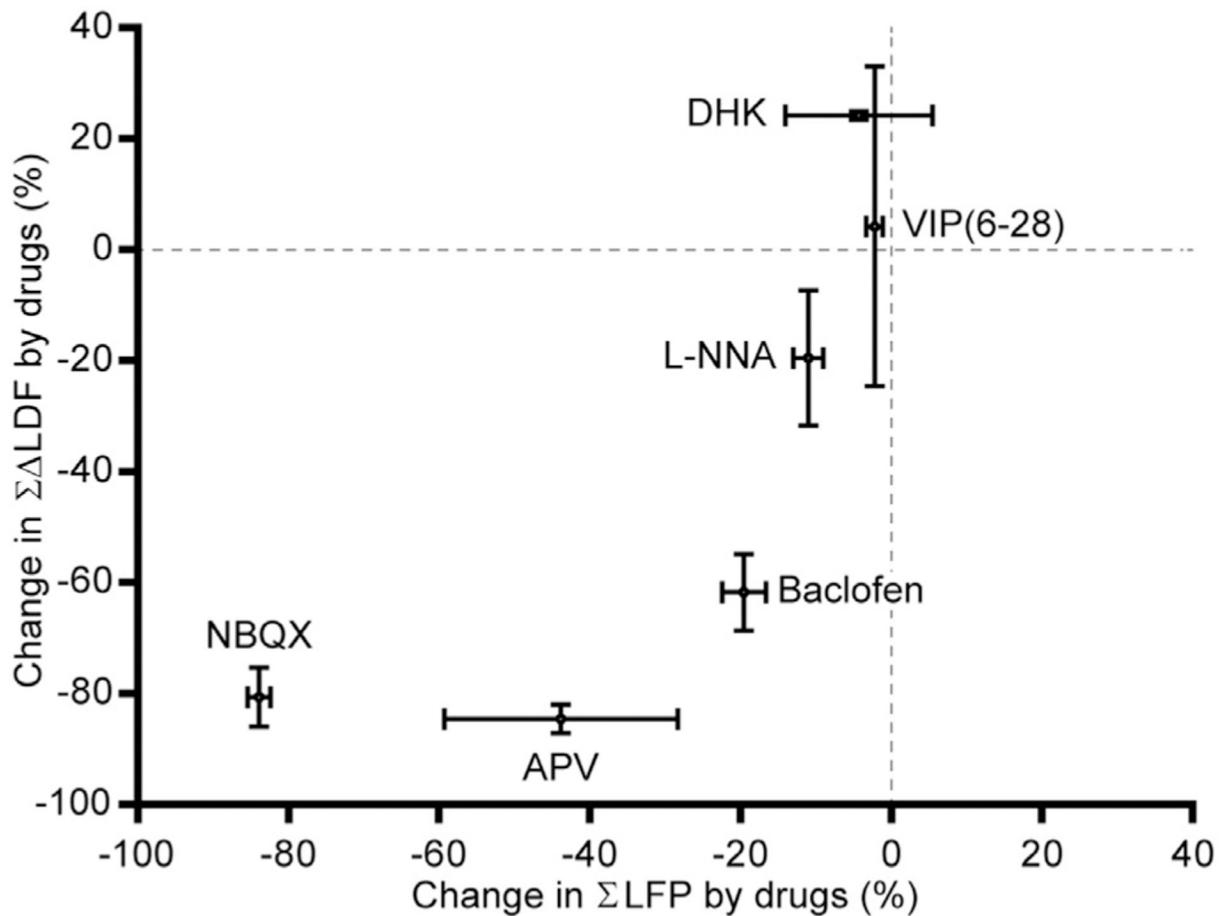


**Fig. 8. Summary of the LFP and blood flow response changes caused by the pharmacological agents.**

Summary of the mean  $\Sigma$ LFP and  $\Sigma$  LDF changes to LOT stimulation during application of the different drugs relative to the pre-drug control period. Interestingly, the AMPA receptor antagonist (NBQX) had a greater effect on the neuronal responses to LOT stimulation compared to the NMDA receptor antagonist (APV), yet the blood flow responses were similar. This may be due to subthreshold neuronal activities (i.e., the slow-rising phase of the exponential relationship) or to calcium-dependent hemodynamic response cascades initiated by NMDA channel openings. Since an exponential relationship can be seen between the  $\Sigma$ LFP and  $\Sigma$  LDF data, similar to the LOT stimulus-amplitude titration curve (Fig. 1F), decreased blood flow responses caused by the GABA<sub>B</sub> receptor agonist (baclofen) may be due to indirect changes in the neuronal network dynamics rather than to direct neurovascular coupling to GABA release.